NASA Technical Memorandum 105209

IN-34
45746

p57

Resonant Triad in Boundary-Layer Stability

Part II. Composite Solution and Comparison With Observations

Reda R. Mankbadi
Lewis Research Center
Cleveland, Ohio

September 1991

NASA

RESONANT TRIAD IN BOUNDARY-LAYER STABILITY

PART II. COMPOSITE SOLUTION AND COMPARISONS WITH OBSERVATIONS

Reda R. Mankbadi

National Aeronautics and Space Administration
Lewis Research Center
Cleveland, Ohio 44135

ABSTRACT

Numerical results are computed from the asymptotic near-resonance triad analysis of part I. The analysis considers a resonant triad of instability waves consisting of a plane fundamental wave and a pair of symmetrical oblique subharmonic waves. The relevant scaling ensures that nonlinearity is confined to a distinct critical layer. The analysis is first used to form a composite solution that accounts for both the flow-divergence and nonlinear effects. It is shown that the backreaction on the plane Tollmien Schlichting (TS) fundamental wave, although fully accounted for, is of little significance. The observed enhancement at the fundamental frequency disturbance is not in the plane Tollmien-Schlichting wave but is caused by nonlinearly generated waves at the fundamental frequency that result from nonlinear interactions in the critical layer. The saturation of the oblique waves is caused by their self-interaction. The nonlinear phase-locking phenomenon, the location of resonance with respect to the neutral stability curve, low-frequency effects, detuning in the streamwise wavenumbers, and nonlinear distortion of the mode shapes are discussed. Nonlinearity modifies the initially two-dimensional Blasius profile into a fuller one with spanwise periodicity. The interactions at a wide range of unstable spanwise wavenumbers are considered, and the existence of a "preferred" spanwise wavenumber is explained by means of the vorticity distribution in the critical layer. Besides presenting novel features of the phenomena and explaining the delicate mechanisms of the interactions, the results of the theory are in excellent agreement with experimental and numerical observations for all stages of the development and for various input parameters.

1. INTRODUCTION

Part I of this study shows how the critical-layer nonlinearity (CLN) controls the nonlinear development of a near-resonance triad of waves in boundary-layer transition. The triad consists of a plane wave at the fundamental frequency ω and a pair of symmetrical oblique waves of a common amplitude at the subharmonic frequency $\omega/2$. The nonlinear viscous dynamics in the critical layer determine the development of the waves. The analysis is fully nonlinear. In addition to the initial input waves in the triad, nonlinear interactions generate other waves of nonlinear amplitudes that were not initially present.

As was shown in part I, in the initial stage of interaction the presence of the plane wave causes an exponential-of-an-exponential growth of the oblique modes. In this stage, which is loosely termed the "parametric resonance stage," the backreaction on the plane wave cancels out, even when the modes are of the same order of magnitude. However, as the amplitude of the oblique waves exceeds a certain level relative to the plane wave, a fully interactive stage is reached in which a backreaction occurs and the growth rates are fully coupled. In this stage the oblique waves also interact with themselves, causing their saturation – a mechanism that is independent of the plane wave.

The development of the instability waves is governed by both the nonlinear effects considered in part I and the nonparallel-flow effects, which are weak because the Reynolds number is asymptotically large. Nonparallel-flow effects occur over a much larger streamwise length scale than nonlinear effects. It is therefore possible to construct a composite solution as was done in Goldstein & Leib (1988) by first considering nonlinearity and then accounting for the non-parallism resulting from the flow divergence. An overview of the nonlinear critical-layer theory developed in part I is presented is §2. The resulting nonlinear amplitude equations are then used to form a composite solution that accounts for both the nonlinear effects and those caused by flow divergence.

The spatial evolution of the waves is presented in §3, where an excellent agreement between theory and experimental data is found over almost all the stages of the development and for a broad range of input parameters. Results are also in good agreement with the numerical simulations that are available for the parametric resonance stage of interaction. The nonlinear self-interaction of the oblique waves produces important two- and three-dimensional waves of nonlinear amplitudes at the fundamental frequency. As the amplitude of the oblique waves increases, the amplitudes of these nonlinearly generated waves become comparable to that of the input Tollmien-Schlichting (TS) plane fundamental wave, which is part of the input triad. Thus, although the TS fundamental wave suffers a slightly steeper decay because of the backreaction, the net fundamental frequency component is enhanced by the nonlinearly generated waves. Thus the self-interaction of the oblique waves is primarily responsible for both the saturation of the oblique waves and the enhanced fundamental growth. The backreaction, although fully accounted for in the theory, is of little practical importance.

The role of the initial disturbance level in nonlinear wave development and saturation is clarified in §3. The occurrence of subharmonic resonance in the vicinity and downstream of the upper branch, with the maximum growth rate occurring not at but downstream of the upper branch, is explained. The nonlinear phase-locking phenomenon, low-frequency effects, and detuning in the streamwise wavenumbers are also discussed in §3.

In §4 the nonlinear effects on the mode shapes and on the mean flow are described. It is shown that nonlinearity causes the initially two-dimensional Blasius profile to become fuller and three-dimensional spanwise periodic. This distortion of the mean flow must be accounted for, as is done in the present analysis, in order to determine the nonlinear spatial development of the triad amplitudes.

2

Most of the computed results correspond to an obliqueness angle of 60°
(which is an ideal resonant condition). However, the analysis is extended in
§5 to study near-resonant conditions. Results indicate that the nonlinear
interaction occurs over a range of spanwise wavenumbers as wide as that pre-
dicted by previous numerical results. The strongest interaction occurs at an
obliqueness angle of about 60°, as observed experimentally. The vorticity dis-
tribution in the critical layer is given to explain the effects of the spanwise
wavenumber.

A discussion and summary are given in §6. It is our contention that the
theory not only reveals intricate details of the interaction mechanisms that
could not be found from previous analyses, but also reveals novel features and
provides new explanations of observed phenomena.

2. COMPOSITE SOLUTION

The overall growth of an instability wave is governed by both nonlinear
and weakly nonparallel flow effects. The results of part I pertain to the non-
linear effects, which are reviewed here. Then the composite solution is given
in §2.2.

2.1. Nonlinear Effects

In part I of this study the nonlinear development of a fully interactive
near-resonance triad was considered. The triad consists of a plane fundamen-
tal wave of frequency ω and a pair of symmetrical oblique waves at the sub-
harmonic frequency $\omega/2$. The streamwise wavelengths of the plane and oblique
waves are α and nearly $\alpha/2$, respectively. The triad starts as spatially
growing, initially linear instability waves.

Experiments on boundary-layer transition have indicated that subharmonic
resonance occurs at low dimensionless frequencies F^* and at Reynolds number
R in the vicinity and downstream of the upper-branch neutral stability curve.
The Reynolds number scales as

$$\bar{R} = \sigma^{10} R \ .$$
(2.1a)

Here an overbar ($^-$) denotes a scaled order-one real quantity. The small fre-
quency parameter σ can be related to the dimensionless frequency by the
relation

$$F^* = \frac{\omega\nu}{U_\infty^2} = \sigma^{12} \ .$$
(2.1b)

The wavenumbers α and γ and the phase velocities c_0 and c of the plane
and oblique waves, respectively, are then scaled accordingly. The waves have
a nearly common critical layer where the mean-flow velocity equals the phase
speed of the waves. Outside the critical layer the flow is governed by linear
dynamics

3

$$u = U_B(y) + \mathcal{R}e\left\{\epsilon A_o(x_1)\,\frac{\partial \Phi_o}{\partial y}\,(y,x_1,\sigma)e^{iX} + \delta A(x_1)\left[U_+(y,x_1,\sigma)e^{iZ}\right.\right.$$

$$\left.\left. + U_-(y,x_1,\sigma)e^{-iZ}\right]e^{iX/2}\right\} \qquad (2.2a)$$

$$v \equiv \mathcal{R}e\; i\left[\epsilon\alpha A_o\Phi_o e^{iX} + \delta\gamma A(e^{iZ} + e^{-iZ})\Phi e^{iX/2}\right] \qquad (2.2b)$$

and

$$w = \delta\mathcal{R}e\, A\left(W_+ e^{iZ} + W_- e^{-iZ}\right)e^{iX/2} \qquad (2.2c)$$

where

$$x_1 \equiv \sigma^4 x\;, \qquad (2.2d)$$

$$X \equiv \sigma\bar{\alpha}(x - \sigma\bar{c}t)\;, \qquad (2.2e)$$

$$Z \equiv \sigma\bar{\beta}z\;, \qquad (2.2f)$$

and

$$\bar{\gamma} \equiv \sqrt{\left(\frac{\bar{\alpha}}{2}\right)^2 + \bar{\beta}^2}\;, \qquad (2.2g)$$

and where x, y, and z are the coordinates in the streamwise, transverse, and spanwise directions, respectively; u, v, and w are the corresponding velocity components; β is the spanwise wavenumber. Here U_B is the Blasius profile, Φ_o and Φ are the eigenfunctions satisfying the linear Orr-Sommerfeld and Squire equations, respectively, and $U_\pm$ and $W_\pm$ are related to the eigenfunction Φ. The amplitude functions for the two-dimensional and oblique waves are given, respectively, by $A_o(x_1)$ and $A(x_1)$, and their measures are ϵ and δ. These amplitudes and their measures are determined by considering the nonlinear viscous flow in the critical layer.

The scaling leads to a linear stability structure in which the critical layer is distinct from the wall layer. Matching the linear solution at the different transverse zones produces a linear relation between the growth rate and the velocity jump ($\Delta\phi$, $\Delta\phi_o$) across the critical layer for each mode

$$\left(\cos\theta + \frac{1}{\cos\theta}\right)\frac{A'}{A} = \frac{(\bar{\gamma}\bar{c})^2}{4\lambda^3}(\Delta\phi) + \frac{\bar{\gamma}^2}{(\bar{c})^2\sqrt{2\bar{c}R\bar{\gamma}}} , \qquad (2.3a)$$

$$\frac{A'_o}{A_o} = \frac{(\bar{\alpha}\bar{c}_o)^2}{8\lambda^3}(\Delta\phi_o) + \frac{\bar{\alpha}^2}{2(\bar{c}_o)^2\sqrt{2\bar{c}_oR\bar{\alpha}}} + i\mathcal{I}m\left(\frac{A'_o}{A_o}\right)_{initial} , \qquad (2.3b)$$

where (') denotes differentiation with respect to the slow variable x_1. The matching also requires

$$\bar{\gamma} = \bar{\alpha} + 2\sigma^3\mathcal{I}m\frac{A'_o}{A_o} , \qquad (2.4a)$$

which for perfect tuning gives an obliqueness angle

$$\theta = \tan^{-1}\frac{\beta}{\frac{\alpha}{2}} \qquad (2.4b)$$

of 60°.

At the critical point the linear solution is singular and therefore needs to be rescaled. The critical-layer scaling is governed by the following criteria: (1) The nonlinear solution develops from a finite-growth-rate, strictly linear stability solution. (2) Nonlinear terms in the critical-layer solution must balance the velocity jump across the critical layer at the same order as in the linear solution. (3) The amplitudes of the oblique waves can reach values large enough for the fully interactive case, in which the oblique waves produce a nonzero backreaction on the plane wave. The analysis indicates that if the modes are of the same order, the backreaction on the fundamental cancels out. The order of magnitude of the oblique waves must exceed that of the plane wave divided by $\sigma^{2.5}$ in order to produce a nonzero backreaction. The appropriate scaling in the critical layer is given by

Transverse coordinate:

$$\bar{\eta} = \frac{y - y_c}{\sigma^3} \qquad (2.5a)$$

Scale of the plane wave:

$$\varepsilon = \sigma^{10} \qquad (2.5b)$$

5

Scale of the oblique waves:

$$\delta = \sigma^{7.5} \tag{2.5c}$$

where y_c is the location of the critical point $U_B = c$. This is also the same one at which the important self-interaction of the oblique waves appears.

The expansion in the critical layer can be written in the general form

$$u - \sigma\bar{c} = \sigma^3\lambda\bar{\eta} + \sigma^{5.5}U_{5.5} + \sigma^6 U_6 + \sigma^{6.5}U_{6.5} + \ldots , \tag{2.6}$$

and a similar expression can be written for the other velocity components, v and w, the pressure p, and the vorticity. The governing nonlinear viscous equations for each level in the expansion are then obtained from Navier-Stokes equations. The Fourier transform is used to solve analytically for each level in the expansion. Within the order of approximation, nonlinearities are confined within the critical layer. The nonlinear solution for each level of the expansion matches the corresponding linear solution outside the critical layer.

In order for the solutions to match, the velocity jump across the critical layer calculated from the nonlinear solution within the critical layer must be equal to the jump calculated from the linear solution outside the critical layer. The amplitude equations are obtained by substituting for the jump calculated from the nonlinear viscous solution into equation (2.3). The analytically obtained scaled amplitude equations for the oblique waves and the plane wave are given, respectively, for $\theta = 60°$ as

$$\frac{dA}{d\bar{x}} = \underbrace{\frac{4}{5} k_o A}_{\text{Linear}} + \underbrace{\frac{3}{10} \pi \frac{\bar{R}^3}{\lambda} iA^*A_o}_{\substack{\text{Mutual} \\ \text{(parametric} \\ \text{resonance)}}} - \underbrace{\frac{2}{5} iM \frac{\bar{R}^{4.5}}{\lambda\sqrt{\lambda}} A^2 A^*}_{\substack{\text{Self-} \\ \text{interaction}}} \tag{2.7a}$$

and

$$\frac{dA_o}{d\bar{x}} = \underbrace{(k_o + ik_i)A_o}_{\text{Linear}} + \underbrace{iM_1 \frac{\bar{R}^{4.5}}{\lambda\sqrt{\lambda}} A_o AA^*}_{\substack{\text{Mutual} \\ \text{(detuning)}}} - \underbrace{iM_2 \frac{\bar{R}^6}{\lambda^2} A^*A^3}_{\text{Backreaction}} , \tag{2.7b}$$

where

$$k_o = \frac{\lambda^2}{2\sqrt{2}\,\bar{R}} - \frac{\pi}{8} \frac{\bar{R}^2}{\lambda^3} , \tag{2.7c}$$

6

and the constants M are calculated analytically as

$$M = M_r + iM_i = 1.055 - i16.8 , \qquad (2.7d)$$

$$M_1 = 0.5848 , \qquad (2.7e)$$

$$M_2 = -0.241 . \qquad (2.7f)$$

The initial detuning factor is k_i, the Blasius skin friction coefficient is $\lambda = 0.332$, and (*) denotes a complex conjugate.

The lowest order solution of the oblique waves is given by

$$U_{5.5} = 2 \tan \theta \cos z \, \mathcal{R}e \left[iQ(\bar{\eta}, x_1) e^{iX/2} \right] \qquad (2.8a)$$

and

$$W_{5.5} = 2 \sin z \, \mathcal{R}e \left[iQ(\bar{\eta}, x_1) e^{iX/2} \right] \qquad (2.8b)$$

where

$$Q = \sin \theta \, A \int_{-\infty}^{0} e^{ik\eta} e^{hk^3/3} \, dk , \qquad (2.8c)$$

$$\eta = \frac{\bar{\eta}}{\bar{c}} , \qquad (2.8d)$$

and

$$h = \frac{2}{\bar{R}^3} . \qquad (2.8e)$$

The critical-layer nonlinearity not only determines the nonlinear development of the triad's waves, but also generates other important waves of nonlinear amplitudes. The lowest order at which these generated waves appear is σ^8, and they are given in appendix B of part I.

2.2. Flow-Divergence Effects

The preceding results pertain to the nonlinear development of the waves when boundary-layer growth is ignored. As has been stated, the overall instability wave growth is dependent on both the nonlinear effects given in the preceding section and the weakly nonparallel flow effects. In order to incorporate both effects into a single formula, Goldstein & Leib (1988) was followed

7

in formulating a composite expansion by using the inner (nonlinear) solution (eqs. (2.7)), A_{in}, and the slowly varying outer (linear) solution, A_{out}. Details of the procedure are given in appendix A, where the final form of the composite solution is obtained as

$$\frac{dA}{dR} = \sigma^4\left(1 + \frac{R_i^2}{R^2}\right)\left[\underbrace{\frac{4}{5} k_o A}_{\text{Linear}} + \underbrace{\frac{3}{10} \pi \frac{\bar{R}^3}{\lambda} iA^*A_o}_{\substack{\text{Parametric}\\\text{resonance}}} - \underbrace{\frac{2}{5} iM \frac{\bar{R}^{4.5}}{\lambda\sqrt{\lambda}} A^2A^*}_{\substack{\text{Self-}\\\text{interaction}}}\right] \qquad (2.9a)$$

with the leftmost factor labeled Divergence.

and

$$\frac{dA_o}{dR} = \sigma^4\left(1 + \frac{R_i^2}{R^2}\right)\left[\underbrace{(k_o + ik_i)A_o}_{\text{Linear}} + \underbrace{iM_1 \frac{\bar{R}^{4.5}}{\lambda\sqrt{\lambda}} A_oAA^*}_{\substack{\text{Mutual}\\\text{(detuning)}}} - \underbrace{iM_2 \frac{\bar{R}^6}{\lambda^2} A^*A^3}_{\text{Backreaction}}\right] , \qquad (2.9b)$$

with the leftmost factor labeled Divergence.

where R_i is the initial Reynolds number. Here A and A_o now denote the composite scaled amplitudes and can be related to the corresponding unscaled amplitudes A_{3D} and A_{2D} by

$$A_{3D} = \sigma^{7.5}A \qquad (2.10a)$$

and

$$A_{2D} = \sigma^{10}A_o . \qquad (2.10b)$$

The complex equations (2.9) can also be recast in terms of a set of real equations in the form

$$\frac{d|A|}{dR} = \sigma^4\left(1 + \frac{R_i^2}{R^2}\right)\left[\frac{4}{5} k_o|A| - d_o \sin(\psi_e)|A_o||A| + d_i|A|^3\right] , \qquad (2.11a)$$

$$\frac{d|A_o|}{dR} = \sigma^4\left(1 + \frac{R_i^2}{R^2}\right)\left[k_o|A_o| - S_2 \sin(\psi_e)|A|^4\right] , \qquad (2.11b)$$

and

$$\frac{d\psi_e}{dR} = \sigma^4\left(1 + \frac{R_i^2}{R^2}\right)\left[k_i + (2d_r - S_1)|A|^2 - \cos(\psi_e)\left(2d_o|A| + S_2 \frac{|A|^4}{|A_o|}\right)\right] , \qquad (2.11c)$$

8

where

$$\psi_e = \psi_o - 2\tilde{\psi} \ , \tag{2.12a}$$

$$S_1 = M_1 \frac{\bar{R}^{4.5}}{\lambda \sqrt{\lambda}} \ , \tag{2.12b}$$

$$S_2 = M_2 \frac{\bar{R}^6}{\lambda^2} \ , \tag{2.12c}$$

$$d_o = 0.3 \ \pi \frac{\bar{R}^3}{\lambda} \ , \tag{2.12d}$$

$$d_r = \frac{2}{5} M_r \frac{\bar{R}^{4.5}}{\lambda \sqrt{\lambda}} \ , \tag{2.12e}$$

$$d_i = \frac{2}{5} M_i \frac{\bar{R}^{4.5}}{\lambda \sqrt{\lambda}} \ . \tag{2.12f}$$

3. SPATIAL EVOLUTION OF WAVES

The analysis suggests that there are two sets of waves. The first set is the input waves in the triad comprising the plane TS fundamental wave of amplitude A_0 and the pair of subharmonic oblique waves of amplitude A. The other set of waves comprises the additional waves generated by the nonlinear interactions in the critical layer. These nonlinearly generated waves are fully accounted for in the present theory. This section describes the spatial evolution of the subharmonic and fundamental waves.

The composite solution (eqs. (2.9)) describes the development of the triad waves that takes into account the nonlinear and flow-divergence effects. The solution of equations (2.9) is governed by the initial amplitudes, the Reynolds number R, the frequency parameter F^*, and the initial detuning factor k_i. The solution is also dependent on the initial phase angles ψ_{oi} and ψ_i. This dependence on the initial phase angles is replaced by dependence on the effective phase angle ψ_{ei} defined in equation (2.12a). Unless otherwise stated, the results presented herein are for $k_i = 0$, $\psi_{ei} = 3\pi/2$, and $\theta = 60°$. The effects of k_i, ψ_{ei}, and θ are discussed in §3.5, 3.6, and 5. In the following, u_{2D} and u_{3D} denote the streamwise velocity transverse maximum in the critical layer of the plane and in the oblique waves, respectively, and u_f denotes that of the net fundamental. Further details are given in appendix B.

3.1. Development of Amplitudes and Detailed Comparisons with Observations

3.1.1. Parametric Resonance Stage

The first stage of the nonlinear interaction, is the "parametric resonance stage," which follows the linear stage and this stage is characterized by superexponential resonant growth of the subharmonic which is caused by the fundamental-subharmonic interaction. If only the parametric resonance and the linear mechanisms were considered in the amplitude equations, while freezing Reynolds number, the subharmonic would grow as the exponential of an exponential, as pointed out in part I. The boundary-layer growth reduces the resonance growth from exponential of exponential to a super exponential.

Figure 1 shows the predicted development of the triad waves at the frequency $F^* = 124 \times 10^{-6}$, where experimental and numerical observations are available for the parametric resonance stage. The results are compared with the experimental data of Kachanov & Levchenko (1984) ($\equiv$KL) under plane wave excitation, where the subharmonic arose from the background disturbance. The computation started at the downstream location where the oblique subharmonic became distinguishable from the background disturbance. The upstream detuned stage is discussed in §3.6. The numerical results of Herbert (1988); Fasel, Rist & Konzelmann (1990); and Crouch (1988) are also shown in the figure. The predictions are generally in good agreement with observations. The subharmonic predicted according to the present theory is slightly closer to the measured data than are previous predictions because of the self-interaction of the oblique waves that is accounted for herein.

3.1.2. Fully Interactive Stage

Corke & Mangano's (1989) ($\equiv$CM) experiments on boundary-layer transition were conducted under carefully controlled phase-coupled input of simultaneous two- and three-dimensional disturbances. This simultaneous wave generation was accomplished by using a spanwise array of line heaters suspended just above the wall at the approximate height of the critical layer in the boundary layer. These heaters were operated to produce, through local heating, time-periodic and spanwise-varying velocity perturbations. Data were obtained for the combined forcing of a fundamental plane wave and a pair of subharmonic oblique waves. The initial conditions of both modes are thus well defined. In previous experiments on ribbon-induced transition the initial level of the plane fundamental was artificially forced to be much higher than that of the oblique subharmonic in the background disturbance. In CM's experiments, however, the initial level of the oblique mode was comparable to that of the plane one, making the experiment resemble more the naturally occurring transition. But most importantly this comparability allowed measurements to be taken in the fully interactive saturation and decay stages, where the oblique waves exceed the plane wave. The experiments revealed novel features of this fully interactive stage that were not available before. Thus, because of CM's well-defined, cleaner initial conditions and wider streamwise measurements, their experimental data provided a rigorous and complete test for evaluating theoretical and numerical investigations.

The amplitudes of the subharmonic and fundamental waves are compared in figures 2 and 3 with Corke & Mangano's (1987, 1989) data at various initial levels and dimensionless frequencies F^*. In each case the initial data points determine the initial levels of the fundamental and the subharmonic as well as the initial Reynolds number for the corresponding computed results. No attempts were made to optimize the initial conditions for best fit with the data. For clarity the discussion of subharmonic and fundamental is separated into two sections.

3.1.2.1. Oblique subharmonic waves. - The comparison between theory and experimental data in figure 2 indicates general overall agreement. The parametric resonance stage is followed by the fully interactive stage. The latter is characterized by a slowing of the superexponential growth of the subharmonic to reach its peak, which is well predicted. Several mechanisms contribute to the saturation and decay of the subharmonic. The dominant one is the self-interaction of the oblique waves, which is discussed in part I of this study. This mechanism always results in a negative growth rate and becomes important as the amplitude of the oblique waves becomes large. Flow divergence causes two other decay mechanisms. The parametric resonance growth of the oblique waves is dependent on the amplitude of the plane wave, which decays beyond the upper branch because of flow divergence. Therefore the parametric resonance mechanism becomes less significant and diminishes farther downstream with the decay of the plane wave. Divergence also causes the linear growth rate of the subharmonic to decrease in the streamwise direction and to ultimately become negative downstream of the upper branch. These nonlinear and divergence effects lead to the predicted saturation and decay of the subharmonic.

Following the subharmonic's saturation, transition to turbulence occurred and the waves decayed. This transition was manifested in CM's data by the loss of linear phase locking, a broadband velocity spectrum, and a fuller mean velocity profile. The decay of the oblique waves is caused by the mechanisms discussed previously. But figure 2 shows that the measured decay rate of the subharmonic is steeper than the predicted one. The experiment indicates an additional decay mechanism resulting from imperfection in imposing the initial forcing in the experiment (CM). The modes nonlinearly phase-locked with the subharmonic's shift toward lower frequencies. The lower frequencies were traced to broad sidebands on the initial fundamental and subharmonic modes and coherent sum and difference modes. Corke & Mangano (1989) surmised the origin of these sidebands to be small imperfections in mode tuning produced by stochastic input from free-stream disturbances. This additional input produced interactions that distributed energy to a broad band of modes, leading to broad spectral filling. The initial spectrum considered in the theory is composed of only the triad waves of discrete frequencies; additional frequencies resulting from imperfections in the experiment are not included. Thus the steeper decay in the experiment was caused by the imperfections in the imposed signal. This difference between the predicted and measured decay rates is important because it distinguishes the decay mechanisms resulting from the interactions of the triad waves and those resulting from imperfections in the imposed initial signal in the experiment. This latter additional decay mechanism has been studied in another experiment reported in Dal-Ferro (1987) and in Corke (1989).

11

<u>3.1.2.2. Fundamental wave</u>. - A distinction is made here between the plane TS fundamental wave in the input triad and the net fundamental disturbance. The latter is composed of the input plane TS fundamental wave plus other waves at the fundamental frequency generated by the nonlinear interactions of the triad waves in the critical layer. These additional waves have two-dimensional as well as three-dimensional spanwise-periodic components that were not originally present in the upstream linear region.

<u>3.1.2.2(a). Plane TS fundamental</u>: As figure 3 shows, both theory and observations indicate that the growth rate of the fundamental is generally slow relative to that of the subharmonic. At later downstream stages, where the subharmonic peaks, the measured fundamental appears to be slightly higher than the predicted plane TS fundamental of amplitude A_{2D}. But CM points out that the measured data at the fundamental frequency in this region were dominated not only by the plane TS wave but also by other nonlinear spanwise-periodic components at the fundamental frequency. Thus, although the backreaction is fully accounted for herein, it has a minimal effect on the plane TS fundamental and cannot explain the experimentally observed enhanced fundamental. The generation of nonlinear waves is discussed next to show that superimposing all waves, linear (input) and nonlinear (generated), at the fundamental frequency explains the observed enhancement in the measured fundamental.

<u>3.1.2.2(b). Nonlinear waves</u>: In the present analysis the velocity in the critical layer expands according to equation (2.6). The oblique waves of amplitude $\sigma^{5.5}A$ interact and produce higher nonlinear waves of amplitude $\sigma^{8}A^{2}$ of the form $(\pm\alpha,\pm2\beta)$, $(\pm\alpha,0)$, $(0,\pm2\beta)$, $(0,0)$. These σ^{8} waves interact with the $\sigma^{5.5}$ waves to produce higher-order nonlinear waves of amplitude $\sigma^{10.5}A^{3}$ of the form $[\pm(3\alpha/2),\pm3\beta]$, $[\pm(3\alpha/2),\pm\beta]$, $[\pm(\alpha/2),\pm3\beta]$, $[\pm(\alpha/2),\pm\beta]$. Also the input plane fundamental interacts with the input oblique subharmonic to produce waves of amplitude $\sigma^{10.5}A_{0}A$ in the form $[\pm(3\alpha/2),\pm\beta]$, $[\pm(\alpha/2),\pm\beta]$. These $\sigma^{10.5}$ waves interact with the $\sigma^{5.5}$ waves to produce higher-order nonlinear waves of amplitudes $\sigma^{13}A^{4}$, $\sigma^{13}A^{2}A_{0}$ in the form $(\pm2\alpha,\pm4\beta)$, $(\pm2\alpha,\pm2\beta)$, $(\pm2\alpha,0)$, $(\pm\alpha,\pm4\beta)$, $(\pm\alpha,\pm2\beta)$, $(\pm\alpha,0)$, $(0,\pm4\beta)$, $(0,\pm2\beta)$, $(0,0)$. All these nonlinear waves are accounted for in the present analysis because some of their interactions control the amplitude equations of the triad's waves.

It is shown herein that nonlinearly generated waves at the fundamental frequency play a crucial role in interpreting the measured data at the fundamental frequency and in clarifying the misconception about the role of backreaction. The nonlinear waves at the fundamental frequency of lowest order, σ^{8}, are given by (see appendix B of part I)

$$U_{8}^{\pm20} = \frac{3}{4} |A|^{2} \frac{\overline{R}^{2.5}}{\sqrt{\lambda}} \left| \overline{U}_{8}^{(20)}(\eta^{*}) \right| \cos\left[X + 2\tilde{\psi} + \frac{\pi}{2} + \phi_{20}(\eta^{*}) \right] , \qquad (3.1a)$$

12

$$U_8^{\pm2+2} + U_8^{\pm2-2} = \frac{3}{4} |A|^2 \frac{\bar{R}^{2.5}}{\sqrt{\lambda}} \cos 2Z \left| \bar{U}_8^{(22)}(\eta^*) \right|$$

$$\times \cos\left[X + 2\tilde{\psi} - \frac{\pi}{2} + \phi_{22}(\eta^*) \right] , \qquad (3.1b)$$

and

$$W_8^{22} + W_8^{2-2} = \frac{\sqrt{3}}{4} |A|^2 \frac{\bar{R}^{2.5}}{\sqrt{\lambda}} \sin 2Z \left| \bar{U}_8^{(22)}(\eta^*) \right|$$

$$\times \cos\left[X + 2\tilde{\psi} - \frac{\pi}{2} + \phi_{22}(\eta^*) \right] , \qquad (3.1c)$$

where $\bar{U}_8^{(20)}(\eta^*)$ and $\bar{U}_8^{(22)}(\eta^*)$ represent the transverse distribution in the critical layer with $\bar{U}_8^{(20}(0) = 0.793$ and $\bar{U}_8^{(22)}(0) = 0.893$. The total unscaled streamwise velocity at the fundamental frequency is therefore given by

$$u_f = 2\sigma^8 \left(U_8^{(20)} + U_8^{(22)} + U_8^{(2-2)} \right) + \sigma^{10} \lambda |A_0| \cos(X + \psi_0) + \ldots \qquad (3.2)$$

The first term in equation (3.2) denotes the nonlinear waves at the fundamental frequency generated by the self-interaction of the oblique waves. The second term in (3.2) denotes the input plane TS fundamental wave. The nonlinear waves are composed of both two-dimensional waves, $U^{(20)}$, and three-dimensional waves, $U^{2\pm2}$, with twice the spanwise periodicity of the input oblique waves. The amplitude of the nonlinear waves is A^2; that of the input plane TS fundamental is A_0. The striking result is that the order of the nonlinear waves is actually lower than that of the input plane TS fundamental. Therefore the former is comparable to, if not larger than, the latter!

Figure 3 shows all the components, input and generated, at the fundamental frequency and their superposition compared with CM's measurement at the fundamental frequency for several test cases. For all these cases the figure shows that at the streamwise locations, where the oblique waves are large, the nonlinear waves become comparable to the input plane TS wave. When all the waves (linear and nonlinear) at the fundamental frequency are superimposed, the net fundamental is now in good agreement with the corresponding measured data. Other higher-order nonlinear waves at the fundamental frequency, not included in the figure, will also contribute to the peak of the calculated net fundamental and make it even closer to the measured one.

Because these nonlinearly generated waves at the fundamental frequency are composed of both plane and three-dimensional waves, the net fundamental is no longer a two-dimensional one. This is demonstrated in figure 4(a), which shows that the net fundamental is initially a plane wave. As the subharmonic peaks downstream, the nonlinear waves are enhanced, causing the net fundamental to increase and to become spanwise periodic. The fact that the apparent increase

13

in the measured fundamental is produced by two- and three-dimensional non-linearities at the fundamental frequency is quite apparent in figure 30 of CM, which is shown here as figure 4(b). The figure shows the spanwise distribution of the measured mode at the fundamental frequency. At the most upstream position the spanwise distribution is almost uniform, indicating the input two-dimensional wave. Farther downstream the spanwise variation becomes pronounced. At the location of the streamwise peak of the fundamental and subharmonic, the minima in the spanwise distribution become quite visible. The spanwise spacing of the observed minima indicates a spanwise wavelength of one-half that of the subharmonic mode. The measured spanwise wavenumber is the harmonic value, $\pm 2\beta$, exactly as predicted herein. The present analysis thus explains the observed spanwise periodicity of the fundamental where it peaks.

Furthermore the present analysis indicates that these nonlinear waves result from the self-interaction of the oblique waves (not from the interactions between the input fundamental and the subharmonic) and therefore that their amplitude is nonlinear in the form A^2. This can also be inferred from CM's data, which indicate that the spatial character and development of the higher nonlinearities are similar to those of the subharmonic. The decrease in the fluctuation maximum at the center span and the movement away from the wall of the u-eigenfunction modulus at the streamwise peak follow that of the subharmonic. This confirms the present finding that the significant nonlinear waves at the fundamental frequency follow from the self-interaction of the oblique waves and that their amplitudes are proportional to A^2. It also lends further support to the present conclusion that the increase in the fundamental results from the nonlinear waves at the fundamental frequency and not from backreaction.

It has been thought that the increase in the measured total fundamental over the corresponding linear growth of the plane TS wave at later downstream stages was due to a backreaction from the subharmonic on the fundamental by which the subharmonic saturated and the fundamental increased. However, as shown by the present analysis and by the experimental data of CM, this increase in the measured fundamental is not in the lane TS fundamental wave but is attributed to the nonlinear waves at the fundamental frequency generated by the self-interactions of the oblique waves.

3.1.3. Comparison with Crouch's (1988) Computations

Crouch (1988) has extended the linear secondary stability analysis of Herbert (1984, 1988) to account for the mutual nonlinear interaction between the three-dimensional secondary mode and the plane primary mode. He decomposes the plane wave component into a basic-flow component and an interaction component. The basic-flow component acts as a parametric excitation for the three-dimensional secondary wave; the interaction component captures the resonance between the secondary and primary waves.

14

The comparison between Crouch's (1988) results and the experimental data (his figs. 4.23 and 4.24) is shown here as figure 5 along with the corresponding predictions of the present critical-layer theory. The differences between the two predictions is attributed basically to the self-interaction of the oblique waves, which is considered in the present theory.

3.2. Role of Backreaction

In the analysis leading to equation (2.9b) the quadratic terms A^2 were fully accounted for, but they were found to produce no velocity jump across the critical layer. Therefore they cancel out and do not influence the amplitude of the plane TS fundamental wave. This is in accordance with Craik's (1971) estimte that this term is of the order $1/R$ of the resonance term and with Craik's (1985) subsequent estimte that the higher order terms in the backreaction may not be negliglble with respect to the quadratic term. Here the next nonzero term in equation (2.9b) is of the form A_0AA^*, but the coefficient of this term is purely imaginary. Therefore it influences only the phase angle, producing a nonlinear detuning of the plane fundamental wave (see eq. (2.11c)). However, because of the nonlinear phase locking (to be discussed in §3.5), such nonlinear detuning has little effect on the nonlinear development of the amplitudes. The next nonzero backreaction term is of the form A^4, and it does alter the amplitude of the plane fundamental wave. But because it is of the quartic type, it influences the development of the plane mode only in its later stages of development, when the amplitude of the subharmonic is large enough. The sign of the coefficient of this term ($S_2 < 0$) and the nonlinear phase locking at resonance (sin (ψ_e) = -1) are such that they cause this backreaction term to reduce the growth rate of the plane fundamental wave.

To clarify the role of backreaction, figure 6 shows the development of the triad's waves under the fully interactive case (eq. (2.9)) compared with its development had the plane TS fundamental been considered to simply follow the linear theory. At resonance ψ_e is phase-locked and sin(ψ_e) = -1. With S_2 being negative the backreaction tends to reduce growth rate and causes a slightly steeper decay of the plane TS fundamental, as figure 6 shows. The backreaction influences the subharmonic only through ψ_e (eq. (2.11c)). But at resonance sin (ψ_e) = -1 and the development of the subharmonic is almost the same whether the backreaction is considered or not. Therefore the backreaction has practically no effect on the saturation and decay of the oblique waves, which are caused by their self-interaction.

The present analysis thus indicates that the backreaction from the oblique subharmonic on the plane TS fundamental is of almost no significance at all. It has practically no effect on the oblique waves, whose saturation is caused by their self-interaction. Only a slightly steeper decay of the plane TS fundamental is caused by the backreaction. The observed enhancement of the measured total fundamental is not a result of the backreaction but is produced by the nonlinearly generated waves at the fundamental frequency, as outlined in §3.1.2.2(b).

The misconception that in the fully interactive stage the higher oblique waves may cause a backreaction on the plane TS fundamental wave, enhancing its growth rate, originated from the earlier data of KL, which showed that the decay of the measured net fundamental is followed by a short increase. In a

private correspondence with Kachanov (1990) regarding the apparent later enhancement in KL's measured fundamental, he pointed out the following: (1) For an "uncontrolled" initial subharmonic an enhancement in the net fundamental appeared, but (a) in this case the subharmonic had a continuous spectrum and (b) at the later stages of the development, where the total fundamental was enhanced, the data on the three-dimensionality of the fundamental were not processed. (2) Under "controlled" subharmonic priming the backreaction on the fundamental was almost negligible, although the subharmonic amplitude reached values as high as 2.4 times that of the fundamental. The main objective of KL's work was to demonstrate the existence of subharmonic resonance, and they did not investigate the latter stages of the development and the backreaction.

Thus KL's data indicate no backreaction under "controlled" conditions and for the "uncontrolled" case the apparent increase in the total fundamental was not identified to be in the plane TS wave because spanwise investigations were not conducted. This issue was clarified by the spanwise measurement of the fundamental in CM's data, which showed that the enhanced total fundamental is three-dimensional spanwise periodic and that the effect of backreaction on the plane TS fundamental is negligible. Careful examination of the initial decay stage in KL's data (in their fig. 2) indicates that the backreaction actually causes a steeper decay rate of the fundamental (see also §3.3.2 herein). The observed enhancement of the total fundamental at the streamwise location where the subharmonic peaks thus does not result from backreaction but is produced by the nonlinear waves at the fundamental frequency that are generated by the self-interaction of the oblique waves, as outlined before. The saturation of the oblique waves is not influenced by the backreaction but is caused by their self-interaction.

The present finding that the backreaction plays a minimal role actually extends the validity range of the linear secondary stability analysis (LSSA) of Herbert (1984, 1988), which is quite general in terms of its ability to consider various initial modes and does not need the approximations of the high-Reynolds-number limit. There the linear stability of three-dimensional waves in the presence of a slowly varying plane TS fundamental wave is considered. Shape assumptions for the modes are made and a Floquet system is solved numerically. Herbert's basic assumption is that the plane fundamental is the dominant mode so that the interactions do not influence either it or the mean flow. This assumption is obviously valid if the amplitude of the oblique mode is much smaller than that of the plane mode but might be questioned as the oblique waves become comparable to the plane wave. This led Spalart & Yang (1987) to conclude that Herbert's model is relevant to ribbon induced transition, where the plane mode is large with respect to the oblique one, but that the model cannot account for all the three-dimensional effects when the two modes are of comparable amplitudes, as in natural transition. The present analysis indicates that in the initial stage of interaction, where the subharmonic is less than or equal to the fundamental, the backreaction cancels out. But most importantly the present analysis also reveals that the backreaction on the plane fundamental is insignificant even when the oblique mode exceeds the plane one. Therefore the plane wave can be considered to follow the linear stability theory even at large amplitudes of the oblique waves. Herbert's LSSA, which

has revealed great potential, can thus be extended to model the natural transition case where the two modes are of comparable amplitudes. But then the important self-interaction of the oblique waves and the mean-flow distortion must be considered.

3.3. Effect of Initial levels

This section describes the effects of initial levels of the input oblique subharmonic and plane fundamental on their development when other parameters are held fixed.

3.3.1. Initial Level of Subharmonic

The effect of the initial level of the subharmonic oblique waves on their development is shown in figure 7. Equation (2.9a) shows that the linear and parametric resonance growth rates are independent of the subharmonic's amplitude. Therefore the initial growth rate of the subharmonic is not dependent on its initial level. As for the peak, it is controlled by the self-interaction of the oblique subharmonic waves. Because this mechanism is proportional to A^3, a higher initial level of the subharmonic causes an earlier saturation, as the figure illustrates. The figure also shows quite an interesting feature, that the subharmonic's peak is independent of its own initial level. This result is consistent with the findings of part I regarding the development of the oblique waves in the absence of the plane wave.

The effect of the initial level of the subharmonic on the plane TS fundamental is negligible, as figure 7 indicates. The effect of the subharmonic on the fundamental appears only when the subharmonic reaches large levels. Because the subharmonic's peak is independent of its initial level, the development of the plane TS fundamental is practically independent of the subharmonic's initial level.

3.3.2. Initial Level of Fundamental

3.3.2.1. Subharmonic. - Figure 8 shows the development of the subharmonic under various initial levels of the plane fundamental. The parametric resonance mechanism causes a super-exponential growth of the subharmonic, with the argument of the exponent proportional to the initial amplitude of the fundamental. Therefore increasing the initial level of the fundamental causes higher resonance growth rates of the subharmonic, as figure 8(a) illustrates. The peak of the subharmonic is reached when this resonant growth is balanced by the self-interaction of the oblique waves. As the initial level of the fundamental increases, the subharmonic's peak increases and its location moves upstream, up to a saturation level.

The data of KL (in their fig. 2) confirm the trend obtained here that the subharmonic increases with the increasing initial level of the fundamental. However, the KL's data in this regard are to be taken only qualitatively because the subharmonic arose from the background disturbance and its initial level was not fixed while that of the fundamental was raised. In CM's bi-modal

17

excitation experiment, they performed a rigorous test on the effect of the initial level of the fundamental on the development of the subharmonic. The subharmonic's initial level was fixed while that of the fundamental was raised. The amplitude of the subharmonic at the centerline was then measured at a fixed downstream axial location (R = 895). The measured streamwise velocity fluctuation of the subharmonic is shown in figure 8(b) along with the corresponding predictions of the present theory. Shown in the figure are only the data before transition to turbulence occurred at the axial measurement location, as determined by CM. The data were taken as a function of the normalized temperature fluctuation, which is taken to be linearly proportional to the initial level of the fundamental. The figure shows that when the initial fundamental is quite small, little effect on the subharmonic is observed. Corke & Mangano (1989) have indicated that past this initial level the subharmonic's amplitude increases exponentially with increasing initial TS level. This exponential behavior is exactly what the present analysis predicts at levels not high enough for the self-interaction of the oblique waves to be important. This exponential increase eventually slows down as the self-interaction of the oblique waves becomes significant with respect to the parametric resonance mechanism. The tendency toward saturation of the subharmonic with further increase in the initial level of the fundamental is apparent in both theory and experiment. Further increase in the level of the fundamental caused transition to occur at the position where measurements were taken.

3.3.2.2. Plane TS fundamental. - The effect of the initial level of the fundamental on its own development is shown in figure 9(a). The initial growth rate of the fundamental is linear and therefore is independent of its initial level. However, the subsequent development of the fundamental is dependent on its initial level. Increasing the initial level of the fundamental causes higher subharmonic levels. Because of the backreaction the higher levels of the subharmonic lead to earlier saturation and steeper decay of the plane TS fundamental wave.

The effect of increasing the initial level of the fundamental on its own development is evident in KL's figure 2, which is shown here as figure 9(b). The figure indicates that the initial growth of the fundamental is independent of its initial level because it follows the linear theory as predicted herein. Considering the subsequent saturation and decay stages, the figure shows that for all initial levels of the fundamental (curves 1 to 5 in KL's fig. 2) the initial decay of the fundamental is steeper with increasing initial level as predicted herein. But farther downstream a slight increase, or just a slowing in the decay rate, is observed at higher levels of excitation (curves 4 and 5 in KL's fig. 2). As stated earlier, this enhancement is not in the plane TS fundamental but in the total fundamental caused by the nonlinearly generated waves at the fundamental frequency.

3.4. Location of Subharmonic Resonance

In the present theory the form of expansion in the critical layer was dictated by an upper-branch scaling leading to a stability structure in which the critical layer is distinguishable and separable from the wall layer. As pointed out in part I, this scaling was supported by the experimental observations, which indicate that resonance occurs in the vicinity and downstream of

18

the upper branch. Further discussions are given here on the dependence of the resonance phenomena on Reynolds number relative to the neutral stability curve.

Figure 10 shows the parametric resonance growth rate of the oblique subharmonic (second term in eq. (2.9a)) as a function of Reynolds number for various initial levels of the fundamental. The figure shows that the parametric resonance mechanism strongly increases with the initial level of the plane fundamental. The amplitude of the plane fundamental increases with Reynolds number up to the upper branch and begins to decay as its linear growth rate becomes negative. However, the subharmonic's parametric resonance growth rate reaches its maximum not at but downstream of the upper branch. The present formulation indicates that the parametric resonance growth rate is dependent on two factors: (1) It is exponentially proportional to the amplitude of the plane wave, which reaches its maximum at the upper branch. (2) It increases with Reynolds number, which increases continuously in the downstream direction. These two factors combined cause the parametric resonance growth rate to be maximum not at but downstream of the upper branch. The location of the maximum moves slightly upstream with increasing initial amplitude of the fundamental, but it always remains in the vicinity and to the right of the upper branch.

The location of the subharmonic resonance with respect to the neutral stability curve is shown in figure 11 for the experimental data of Kachanov & Levchenko (1984), Saric, Kozlov & Levchenko (1984), and Corke & Mangano (1989). The observed location of the beginning of subharmonic resonance is marked by (o) for each experiment. This location is defined as the point where the observed subharmonic's growth rate is higher than the linear growth rate. Also shown in the figure is the location of subharmonic maximum growth rate (•) as measured by CM. The data in figure 11 clearly indicate that the parametric resonance mechanism becomes important at high Reynolds number in the vicinity of the upper branch, as postulated earlier herein. Thus the upper-branch stability structure adopted here is the appropriate one.

3.5. Nonlinear Phase Locking

In the results presented so far the initial phase difference angle ψ_{ei} (eq. (2.12a)) was taken to be $3\pi/2$. It is well known that in free shear flows the initial phase difference between the fundamental and subharmonic modes can result in either growth or damping of the subharmonic (see, e.g., Zang et al., 1984; Mankbadi, 1985, 1986, and 1991; and Monkewitz, 1988). Zhang & Krist (1989) have also shown that this phase difference may be important in plane channel flow. This issue is rarely addressed in the case of boundary-layer transition, and therefore it is studied herein. Figure 12(a) shows that for all phase angles ψ_{ei}, except those near $\pi/2$, the subharmonic resonates with almost the same strength as for $3\pi/2$. If $\psi_{ei} = \pi/2$, the subharmonic initially decays until ψ_e develops and locks into the optimum value of $3\pi/2$ and then the subharmonic resonates. The peak of the subharmonic is independent of the initial phase difference. The effect of ψ_{ei} can be understood by noting that in equations (2.11) the moduli of the amplitudes are dependent on the phase angles through $\sin \psi_e$. If $\sin \psi_e$ is negative, resonance occurs; and if it is positive, suppression occurs. The development of ψ_e at various initial values ψ_{ei} is shown in figure 12(b). The figure shows that ψ_e develops from its initial value until it nonlinearly locks into an optimum value of

$3\pi/2$. At $\psi_{ei} - \pi/2$, $\sin \psi_e$ is initially positive, causing the subharmonic to decay until $\sin \psi_e$ reverses sign farther downstream and results in the delayed subharmonic resonance shown in figure 12(a).

The effect of the initial phase-difference angle on the fundamental is shown in figure 12(c). The subharmonic influences the fundamental only when the amplitude of the former is higher than that of the latter. By that location ψ_e has already locked into its optimum value, and the subharmonic reaches a peak that is independent of ψ_{ei}. Therefore the development of the fundamental is practically independent of ψ_{ei}.

Why has the suppression of the subharmonic at $\psi_{ei} - \pi/2$ not been experimentally observed? This question is answered in figure 13, which shows the effect of ψ_{ei} on the subharmonic at $R - 825$ (where the subharmonic was minimum in fig. 12(a)). The detuning factor was taken to be zero in figure 12, but it is now considered in figure 13. The figure shows two important features. The first is that the effect of ψ_{ei} is restricted to a narrow window around $\pi/2$. Away from this window the subharmonic growth is almost indistinguishable from that occurring at the optimum $\psi_{ei} - 3\pi/2$. The other important feature in the figure is that the dip occurring at $\pi/2$ is quite sensitive to the detuning factor. At $\psi_{ei} - \pi/2$ the nonlinear phase locking of ψ_e to $3\pi/2$, as well as the subharmonic's resonance, occurs earlier with detuning. The suppression of the subharmonic at $\pi/2$ is therefore drastically reduced with infinitesimal detuning. Perfect tuning can never be achieved in experiments and a small detuning in inadvertently present. Thus because of imperfection in tuning and because it is restricted to a narrow window, the subharmonic suppression at $\psi_{ei} - \pi/2$ can hardly be detected in experiments. This is consistent with the experimental finding of Corke (private communication, 1990) that changing the initial phases of the plane fundamental and oblique subharmonic waves had little effect on the subharmonic resonance.

Attempting to study the effect of the initial phase difference on resonance, Saric et al. (1984) excited a boundary layer at a plane fundamental wave and a plane subharmonic wave while varying the input phase difference between the two waves. The input phase angle in this experiment (both modes are plane waves) influences, but is different from, the effective phase angle ψ_{ei} discussed herein. Their results at difference phase angles are presented in figure 14 along with the corresponding theoretical predictions. The comparison here is to be taken only qualitatively because of the difference in the definition of the phase angles just stated and also because the input spectra in their experiment contained waves at other frequencies of amplitudes comparable to that of the fundamental and subharmonic waves. However, the observations do show weak dependence on the initial phase angle, as predicted herein.

3.6. Wavenumber Detuning

Perfect tuning ($k_i - 0$) requires the wavenumbers' end frequencies to be precisely those of the fundamental and subharmonic values for exact resonance. Because this may not always be the case, the effect of the detuning factor k_i is considered herein.

KL presented two sets of data (their figs. 13 and 23) both at frequency $F^* - 124\times10^{-6}$ and at roughly the same initial levels. In the first set of

data, only a two-dimensional wave at fundamental frequency was imposed while the subharmonic grew up from the background noise. Under such conditions one expects the detuning to be considerably large. For such large detuning the subharmonic hummed before it resonated. In the second set of data KL attempted to reduce the detuning by imposing a second two-dimensional wave at the subharmonic frequency (the detuning was still not quite zero because the imposed subharmonic was a two-dimensional, not a three-dimensional one). As a result of reducing the detuning the hum was reduced and the resonance occurred earlier. These data of KL are shown here in figure 15 along with the corresponding theoretical predictions. Unlike the experiment the initial level of the subharmonic in the computations was fixed in order to isolate the effect of detuning from that of the initial amplitude. The theory predicts the same behavior as in the experiment. At large detuning the subharmonic will hum before it resonates. The location of resonance moves downstream with increasing detuning. Nevertheless the ultimate peak of the subharmonic is almost independent of the initial detuning.

This effect of wavenumber detuning can be explained by noting that it influences the modulus of the subharmonic's amplitude (eq. (2.11(a))) through the effective phase angle $\sin \psi_e$. This angle is shown here in figure 15(b), which indicates that if perfect tuning is initially achieved, ψ_e remains at its optimum initial value of $3\pi/2$, allowing resonance to occur immediately. At high detuning ψ_e deviates from the optimum value, reversing the trend and causing the initial suppression of the subharmonic. But ψ_e develops downstream until it locks into a value close to the optimum one, allowing resonance to occur farther downstream. The main effect of detuning is thus to move in the downstream direction the location where phase locking occurs and thus to shift the resonance location downstream. This interpretation is consistent with Saric et al.'s (1984) observation that in the case of subharmonic arising from the background, as in high initial detuning, a longer fetch (distance from the vibrating ribbon) is required to phase lock and entrain the subharmonic from the background.

Thus the triad's waves do not have to be perfectly tuned in order for resonance to occur. The present theory is applicable to exact-resonance or near-resonance conditions. In order for resonance to occur within a finite streamwise length, the oblique waves need to be only near, not precisely at, the subharmonic value. This conclusion is also supported by the measured spectra of KL (their figs. 4 and 28), which indicate that resonance occurs not in a discrete subharmonic frequency but in a band of frequencies around the subharmonic value. This is also consistent with Santos & Herbert's (1986) finding that the growth rates for the detuned modes show a broad peak in the neighborhood of the subharmonic mode.

The effect of detuning on the modulus of the plane wave amplitude is practically negligible (not shown herein). As pointed out before, the back-reaction on the fundamental is proportional to A^4 and occur farther downstream after the phase locking has already been achieved. Because the subharmonic reaches a value that is independent of detuning, the modulus of the plane wave amplitude is not affected by detuning.

3.7. Effect of Frequency

In many flows of technological importance, such as in flight, the velocity and the Reynolds number are large and the dimensionless frequencies F^* are small. Therefore the present theory emphasizes the low-frequency domain, which may not be easily accessible to either experimental or numerical investigations. Most of the results presented here are at frequency $F^* = 80 \times 10^{-6}$, which is roughly the lowest frequency where resonance has been observed experimentally. The figures were repeated for $F^* = 10 \times 10^{-6}$ but are not shown herein for conciseness. The behavior at $F^* = 10 \times 10^{-6}$ was found to be qualitatively the same as that at $F^* = 80 \times 10^{-6}$, except for the parametric resonance growth rate, which is discussed herein. The maximum growth rate of the subharmonic as a function of the frequency is shown in figure 16(a). The figure illustrates the strong dependence of the parametric resonance mechanism on the dimensionless frequency F^*. The lower the frequency, the stronger the parametric resonance mechanism. At high frequencies the linear growth rates are small and the unstable range is narrow, and therefore the amplitude of the plane wave cannot reach values large enough to trigger subharmonic resonance.

This strong dependence of subharmonic resonance on frequency is not readily available in the experimental data. There is no experiment in which the frequency has been varied systematically while the other controlling parameters were held fixed. However, the trend can be qualitatively observed by surveying the measured maximum amplitude of the subharmonic in available data at different frequencies, which are shown here in figure 16(b). Although such data are to be taken only qualitatively because other initial conditions were not fixed, yet the general trend of the strong dependence of subharmonic resonance on frequency is quite evident in the figure. Therefore the present results regarding the resonance triad mechanism are even more significant to transitions occurring at low dimensionless frequencies.

This strong dependence on the frequency explains the success of the present analysis in predicting results in broad agreement with observations. Although an asymptotic analysis is exact in the limit of the small parameter equals zero, it is of no use unless it is valid at finite values of the small parameter. For example, the boundary-layer theory is an asymptotic solution exact only at infinite Reynolds number, but it is still valid and quite useful at finite Reynolds numbers. The validity range of an asymptotic analysis can be established from comparison with experiments or exact solutions. The present asymptotic analysis is exact when the small frequency parameter is zero. But it is still valid at small finite F^*. Hultgren (1987) has shown that linear asymptotic solutions are valid at $F^* < 10^{-3}$. At high frequencies the present analysis could be less accurate. But the highest reported frequency of observed subharmonic resonance is given by KL as $F^* = 137 \times 10^{-6}$. This value is well within the range of validity of the asymptotic approach, which explains the strong agreement between theory and experiments. As outlined here, the parametric resonance mechanism is quite weak at higher frequencies. The analysis is therefore highly accurate where the phenomenon is significant (smaller F^*) and becomes less accurate at larger F^*. But if F^* is large enough for the analysis to become less accurate, subharmonic resonance would not occur either. The low-frequency asymptotic approach adopted herein is therefore applicable to the entire range of observable subharmonic resonance.

22

4. NONLINEAR EFFECTS ON TRANSVERSE PROFILES

As pointed out earlier, the nonlinear interactions among members of the triad generate other oscillating and nonoscillating components. The effects of these nonlinearities on the mode shapes and on the mean flow are presented here.

4.1. Mode Shapes

The critical-layer nonlinearity modifies the transverse distribution of the oblique subharmonic mode as well as that of the plane fundamental mode. This fact is illustrated by considering the subharmonic's streamwise velocity component in the critical layer:

$$u_s = |A|\cos z \, \mathcal{Re}\left[\left(\sigma^{5.5} \frac{3\bar{R}}{2^{1/3}} i I_{s1}(\eta^*) + \sigma^{7.5} 4\lambda\right.\right.$$

$$\left.+ \sigma^{10.5} \frac{2\bar{R}^{3/2}}{\lambda^{5/2}} I_{s2}(\eta^*)\right) e^{[i(x/2)+\tilde{\psi}]}\right]$$

$$+ \left|A_o\right| |A| \sigma^{10.5} \cos z \, \mathcal{Re}\left[\frac{3}{2} \frac{\bar{R}^{2.5}}{\sqrt{\lambda}} i I_{s\eta}(\eta^*) e^{[i(x/2)+\psi_o+\tilde{\psi}]}\right]$$

$$+ \left[0(\sigma^{10.5}A^3)\right] + \ldots \tag{4.1}$$

where

$$\eta^* = \sqrt{\lambda\bar{R}} \, (y - y_c)/\sigma^3 \tag{4.2a}$$

and

$$y_c = \frac{\sigma}{\lambda}\sqrt{\frac{R}{\lambda}} \quad . \tag{4.2b}$$

The first square-bracketed term in equation (4.1) is the linear viscous profile of the input oblique subharmonic waves. It is dominated by the lowest order term in the bracket, where I_{s1} is given by

$$I_{s1} = \int_0^\infty e^{-ix\eta^*-x^3/3} \, dx \quad . \tag{4.3a}$$

23

The second square-bracketed term in equation (4.1) is the nonlinear distortion of the profile resulting from the fundamental-subharmonic interaction, where

$$
I_{s3} = \int_0^\infty \int_0^\infty e^{-2x_1^3} x_1 \; \cos x\eta \left[e^{-x^3/3} + H(x_1 - x)e^{x^3/3} \right]
$$

$$
+ \; i \; \sin x\eta^* \left[-e^{-x^3/3} + H(x_1 - x)e^{x^3/3} \right] dx_1 \; dx \; . \qquad (4.3b)
$$

The next square-bracketed term in equation (4.1) results from self-interaction of the oblique waves, and it has little effect on the profile.

The subharmonic's profile is shown in figure 17. The dashed line in figure 17(a) is the linear profile; the solid line is the nonlinear profile (eq. (4.1)). The figure illustrates how the nonlinearity distorts the profile, and it shows that this effect is concentrated around the critical point. The profile scales with η^* (eq. (4.1)), which is a function of R and the frequency parameter σ. The unscaled critical-layer thickness in terms of the physical coordinate y is thus reduced with increasing Reynolds number or with reduced dimensionless frequency F^*. Thus direct numerical simulation of boundary-layer transition is even more difficult in the low-frequency, high-Reynolds-number domain. The calculated nonlinear profile of the subharmonic is shown in figure 17(b) along with the corresponding data of CM, and the comparison seems to be satisfactory.

4.2. Mean Flow

The basic mean flow at the beginning of interactions is the two-dimensional Blasius profile. Nonlinearities contribute to the mean flow at several levels. The first effect on the mean flow appears at the σ^8 level, where nonlinearities of the form (0,0) and (0,±2β) rectify the mean flow. The next effect on the mean flow appears at the σ^{13} level in the form (0,0), (0,±2β), (0,±4β). How the lowest-order effects at the σ^8 level influence the mean flow is not discussed here.

The scaled contribution to the mean flow at the σ^8 level is given by

$$
U^{02} + U^{0-2} = \sqrt{\tfrac{3}{\lambda}} \; \bar{R}^{2.5} |A|^2 \cos 2Z \; \mathcal{R}e \left[\bar{U}^{(02)}(\eta^*) \right] \; , \qquad (4.4a)
$$

$$
U^{00} = \sqrt{\tfrac{3}{\lambda}} \; \bar{R}^{2.5} |A|^2 \; \mathcal{R}e \left[\bar{U}^{(02)}(\eta^*) \right] \; , \qquad (4.4b)
$$

$$
W^{02} + W^{0-2} = \tfrac{1}{2}\sqrt{\tfrac{3}{\lambda}} \; \bar{R}^{2.5} |A|^2 \sin 2Z \; \mathcal{R}e \left[\bar{W}^{(02)}(\eta^*) \right] \; , \qquad (4.4c)
$$

24

and

$$V^{02} + V^{0-2} = \frac{3}{4} \frac{1}{\sqrt{\lambda}} \bar{R}^{2.5}|A|^2 \cos 2Z \, \mathcal{Re}\left[\bar{V}^{(02)}(\eta^*)\right] . \qquad (4.4d)$$

The functions $\bar{U}^{02}(\eta^*)$, $\bar{V}^{02}(\eta^*)$, and $\bar{W}^{02}(\eta^*)$ determine the profiles in the critical layer and are obtainable from the integrals in appendix B of part I. Owing to these generated mean-flow nonlinearities, the streamwise mean-flow velocity is no longer the Blasius profile but is now given by

$$U = U_B + \sigma^8|A|^2\bar{R}^{2.5}\sqrt{\frac{3}{\lambda}}\,(1 + \cos 2Z)\,\mathcal{Re}\left[\bar{U}^{(02)}(\eta^*)\right]$$

$$+ O(\sigma^{13}|A|^2) + \ldots , \qquad (4.5)$$

which indicates that nonlinearity modifies both the transverse and the spanwise distributions of the mean flow.

The calculated modified mean-flow profile is shown in figure 18 along with the initial Blasius profile. The initial condition is the same as that of CM's test case at $F^* = 79\times10^{-6}$. The figure shows that as the nonlinearity becomes important downstream, it alters the transverse distribution of the mean flow by producing a kink around the critical point. Relative to the initial Blasius profile, the nonlinearity increases the profile beneath the critical point and reduces it above the critical point. The effect thus tends to produce a fuller profile, and it signals the beginning of change from the laminar to the fuller turbulent profile. The data of CM in their figure 18 also indicate that downstream the mean-flow profile deviates from the Blasius profile to a fuller profile, as predicted herein. The nonlinear terms in equation (4.4) alone cannot explain the complete change from the Blasius profile to the turbulent profile. Nevertheless these nonlinear terms influence the mean flow in the proper direction toward making it a fuller turbulent type of profile.

A quite interesting feature of the nonlinear contribution to the mean flow is the components $U^{0\pm2}$, which produce spanwise periodicity in the mean flow. Figure 19(a) shows the spanwise distribution of the mean flow at $y = 1.2$ for several streamwise locations. The figure shows that owing to the nonlinearly generated components, $U^{0\pm2}$, a spanwise periodicity in the mean flow develops. CM's data have also shown that because of nonlinearity a spanwise periodicity in the mean flow develops. Their figure 31, shown here as figure 19(b), indicates that the boundary-layer displacement thickness varies periodically in the spanwise direction by as much as 10 percent of its spanwise average. The measured spanwise periodicity in the mean flow is 2β, as predicted herein.

Thus nonlinearity not only produces a fuller mean velocity profile but it also causes spanwise periodicity in the mean flow. Therefore an initially two-dimensional Blasius boundary layer that is undergoing transition encounters nonlinearity that modifies it to ultimately become a three-dimensional turbulent one. This mean-flow modification influences the wave development and

25

should therefore be considered in deriving the amplitude equations, as is done herein.

5. INTERACTION AT VARIOUS SPANWISE WAVENUMBERS

Results presented so far pertain to an obliqueness angle θ of 60°. This choice was dictated by the dispersion relation (2.4) under perfect tuning conditions for exact resonance. In KL's data, resonance occurs at $\theta = 63°$. In CM's data, resonance occurs at $\theta = 59°$. These observed values are quite close to the optimum one of $\theta = 60°$ predicted herein. However, CM's data have also shown that subharmonic resonance can occur at other obliqueness angles but with a weaker growth rate than that for $\theta = 60°$. This dependence on the obliqueness angle has also been indicated in the secondary stability analysis of Herbert (1988) and in the direct numerical simulation of Spalart & Yang (1987). Therefore it is of interest to examine how the present critical-layer theory predicts and interprets such dependence on the obliqueness angle.

At $\theta = 60°$ the phase velocities and the critical points of the plane and oblique waves are identical, and the two critical layers exactly coincide. At other angles the phase velocities and critical points are different, but the two critical layers can still overlap considerably. The critical layer here is not too thin, and as will be shown in §5.2 the peaks of the vorticity distributions are shallow. Therefore dependence of the phase speeds on the obliqueness angle is taken care of herein while the critical layers are still considered to be nearly common. For moderate changes of the obliqueness angle from $\theta = 60°$ the amplitude equations (2.9) are generalized in the form

$$\frac{dA}{dR} = \sigma^4 \left(1 + \frac{R_i^2}{R^2} \right) \left[k_{oq} A + \sin^2\theta \, \frac{\pi \bar{R}^3}{\lambda} \, iA^* A_0 - iM(\theta) \, \frac{\bar{R}^{4.5}}{\lambda \sqrt{\lambda}} \, A^2 A^* \right] \Bigg/ \left(\cos\theta + \frac{1}{\cos\theta} \right) ,$$

$$(5.1a)$$

and

$$\frac{dA_0}{dR} = \sigma^4 \left(1 + \frac{R_i^2}{R^2} \right) \left[(k_0 + ik_i)A_0 + iM_1(\theta) \, \frac{\bar{R}^{4.5}}{\lambda \sqrt{\lambda}} \, A_0 AA^* - iM_2(\theta) \, \frac{\bar{R}^6}{\lambda^2} \, A^* A^3 \right] \qquad (5.1b)$$

where

$$k_{oq} = \frac{\lambda^2 \sqrt{\cos\theta}}{\bar{R}} - \frac{\pi}{8} \frac{\bar{R}^2}{\lambda^3 \cos\theta} . \qquad (5.2)$$

The obliqueness angle θ is related to the wavenumbers by equation (2.4b), and $M(\theta)$, $M_1(\theta)$, and $M_2(\theta)$ are now functions of θ as outlined in part I of this study. If θ is different from 60°, a detuning factor k_i is required in order to satisfy the dispersion relation (2.4a). This factor can be written in terms of a fraction k^+ of the scaled streamwise wavenumber α as

26

$$k_i = (\sigma)^{-3}\bar{\alpha}k^+ \ . \tag{5.3}$$

Then k^+ is related to the obliqueness angle by

$$k^+ = \frac{1}{2\cos\theta} - 1 \ . \tag{5.4}$$

Figure 20 shows that the present theory predicts nonlinear development of the subharmonic at $\theta = 45°$, in good agreement with the corresponding data of CM. Comparing figure 20 for $\theta = 45°$ with figure 2, where $\theta = 60°$, shows that resonance occurs farther downstream when the obliqueness angle deviates from $60°$. The same trend is also evident in CM's figure 17.

The effect of u_{2Di} on the maximum parametric resonance growth rate, shown in figure 21, is qualitatively the same as that predicted by the linear secondary stability analysis (Herbert, 1988). With increasing u_{2Di} the growth rates increase, the peak shifts to a higher spanwise wavenumber (larger obliqueness angle), and the range of unstable spanwise wavenumbers is extended. The increase of the resonance growth rate with u_{2Di} follows directly from the dependence of the resonance term on A_0. The shift to a higher spanwise wavenumber and the broader range of unstable spanwise wavenumbers are explained later in §5.2 by the overlapping of the critical layers. The resonance growth rate is zero at $\beta = 0$. This indicates that there is no resonance interaction between a plane fundamental and a plane subharmonic ($\beta = 0$). Thus vortex pairing, which has been observed in free shear flows with inflectional velocity profile (see, i.e., Ho & Huang, 1982; Mankbadi, 1985; and Zaman & Hussain, 1980), is suppressed herein. The present theory indicates that the resonance interaction term (second term in eq. (5.1a)) is proportional to $\sin^2\theta$. Therefore at $\beta = 0$, $\sin\theta = 0$ and there is no resonance interaction. The resonance interaction results from the interaction of the v component of the plane wave at the σ^8 level with that of the oblique subharmonic wave at $\sigma^{5.5}$ level. The corresponding lowest order in a plane subharmonic is not $\sigma^{5.5}$ but σ^8, and therefore the resonance interaction term vanishes at $\beta = 0$. This result is consistent with Nayfeh & Bozatli's (1979) finding that much larger amplitudes (greater than 20 percent of the mean velocity) are required before interactions will occur between plane fundamental waves and plane subharmonic waves in boundary layers.

The effect of spanwise wavenumber on the maximum growth rate of the subharmonic is shown in figure 22 in comparison with observations. In figure 22(a) the maximum total growth rate of the subharmonic as a function of the spanwise wavenumber is compared with the corresponding experimental data of CM. In figure 22(b) the maximum parametric resonance growth rate is compared with the results of the linear secondary stability analysis of Herbert (1988) as well as with the temporal direct numerical simulation of Spalart & Yang (1987), where the amplitude of the plane wave was artificially fixed in the downstream direction. The figure illustrates that in the present critical-layer theory the interaction is not limited to a narrow band of spanwise wavenumbers, but occurs over a range of unstable spanwise wavenumbers as wide as that indicated by the experimental or numerical observations.

5.1. Craik and Herbert Types of Instability Mechanism

Saric & Thomas' (1984) and Saric, et al.'s (1984) experimental observations on boundary-layer transition under plane-wave excitation have indicated certain dependence of the observed spanwise wavenumber on the forcing amplitude. The observed spanwise wavenumber was $\beta/(\alpha/2) = 1.37$ ($\theta = 55°$) at a low forcing level. But $\beta/(\alpha/2)$ increased to 2.92 ($\theta = 70°$) at an intermediate forcing amplitude. They interpreted the first as corresponding to a C type (for Craik) of instability mechanism and the second to an H-type (for Herbert) of instability mechanism. The present critical-layer theory can explain these observations without the need to distinguish between a C or H type of mechanism.

The subharmonic's maximum total growth rate as a function of the spanwise wavenumber normalized by the peak value is shown in figure 23 for low and intermediate initial levels of the plane wave. The figure shows two interesting features. The first is the shift of the peak spanwise wavenumber β_p to a higher value with increasing u_{2Di}. The total growth rate of the subharmonic is governed by both the linear and the parametric resonance mechanisms. The former is maximum if the spanwise wavenumber is zero; the second is maximum at a higher spanwise wavenumber. If u_{2Di} is low enough so that the linear mechanism is important, then β_p is small. As u_{2Di} increases, the parametric resonance mechanism becomes more important and β_p shifts to a higher value. The second feature in figure 23 is that for the low u_{2Di} the growth rates in the range $\beta < \beta_p$ are close to the peak value, but in the range $\beta > \beta_p$ the growth rates rapidly decrease with increasing β. At the higher value of u_{2Di} the trend is reversed. The amplification rates in the range $\beta < \beta_p$ decrease rapidly with decreasing β. But in the range $\beta > \beta_p$ the growth rates are close to the peak value. Thus at the lower forcing level resonance is more likely to occur in the spanwise range $\beta \leq \beta_p$. At the higher forcing level the trend is reversed and resonance is more likely to occur in the range $\beta \geq \beta_p$. The actually observed spanwise wavenumber would thus be sensitive to how the initial subharmonic's level varies with β.

This interpretation, that the observed spanwise wavenumber would depend on the spanwise content of the initial level of the oblique wave, is evident in the data of CM. They showed that maximum resonance occurs at $\theta = 60°$. But resonance can also be observed to occur at another obliqueness angle by increasing the initial level of oblique waves at the spanwise wavenumber corresponding to this angle. Spalart & Yang's (1987) numerical simulations of a boundary layer excited by a plane fundamental wave also show a similar trend. At low amplitudes, u_{2Di}, their calculated subharmonic's spectra show a sharp peak at $\beta = 0.14$ ($\beta/(\alpha/2) = 1.33$, $\theta = 54°$). When they increased the amplitude of excitation to about 1 percent, the sharp peak at $\beta/(\alpha/2) = 1.33$ was still present, but the spectrum was broad and a swelling at higher spanwise wavenumbers around $\beta/(a/2) = 2.38$ ($\theta = 67°$) also appeared. Up to $u_{2Di} = 1$ percent, this broad growth did not catch up with the localized peak at the smaller spanwise wavenumbers. Therefore Spalart & Yang (1987) have concluded, and the present results also indicate, that the observable spanwise wavenumber would depend on the initial noise level.

Another factor that should be considered in interpreting the results of Saric et al. (1984) is the excitation Reynolds number. Compared with other experiments on subharmonic resonance, the location of the excitation mechanism

28

in Saric et al.'s (1984) test facility was farther to the right of the upper branch. It is shown herein that the parametric resonance mechanism increases with R^3 (eqs. (2.9a)) and that the linear mechanism decreases with Reynolds number downstream of the upper branch. Thus the relative importance of the parametric resonance mechanism, with respect to the linear one, increases with Reynolds number. The peak spanwise wavenumber for the former is higher than that for the latter. Therefore in experiments with high excitation Reynolds numbers, as Saric et al. (1984), it is quite possible to observe resonance at higher spanwise wavenumbers. Their observations can thus be explained from the dependence of the linear and parametric resonance mechanisms on u_{2Di} and on the initial Reynolds number.

The distinction between a C type of mechanism and an H type of mechanism that was first proposed by Saric et al. (1984) is not clear from the present CLN concept. Kachanov (1987) points out that there is no convincing evidence of difference between the two, C and H, mechanisms. The two correspond to the subharmonic resonance phenomenon, and both are theories trying to describe the same phenomenon. Craik (1985) has also surmised that "the suggestion of qualitatively different 'C-type' and 'H-type' mechanisms in boundary layers does not yet seem firmly established."

5.2. Vorticity Distribution

The dependence of subharmonic resonance on the spanwise wavenumber can be understood by considering the vorticity distribution in the critical layers. The vorticity of the plane wave is given by

$$\frac{\partial u}{\partial \eta} = - \frac{\sigma^{13}\bar{R}^2}{2^{7/3}\lambda^2} \, Re \; i I_{vf} A_o e^{ix/2} + \ldots , \tag{5.5}$$

whereas that of the oblique waves is given, for $z = 0$, by

$$\frac{\partial u^+}{\partial \eta} = Re \left[\left(2^{1/3} \sin^2\theta \, \sigma^{5.5} I_{v1} - \frac{\sigma^{10.5}}{2^{7/3}\lambda^2} i I_{v2} \right) \bar{R}^2 A e^{ix/2} \right]$$

$$+ Re \left(\frac{\sin^2\theta}{2^{1/3}} \bar{R}^3 \sigma^{10.5} A_o A^* I_{v3} e^{ix/2} \right) + \ldots , \tag{5.6}$$

where

$$I_{vf} = \int_0^\infty e^{-x^3/6 - ix\eta^*} dx , \tag{5.7a}$$

$$I_{v1} = \int_0^\infty x e^{-x^3/3 - ix\eta^*} dx \; , \tag{5.7b}$$

$$I_{v2} = \int_0^\infty e^{-x^3/3 - ix\eta^*} dx \; , \tag{5.7c}$$

$$I_{v3} = \int_0^\infty \cos x\eta^* e^{-x^3/3} dx \; . \tag{5.7d}$$

The vorticity distributions in the critical layers are shown in figure 24 for several obliqueness angles corresponding to different spanwise wavenumbers. The distribution of the vorticity is plotted in terms of the unscaled coordinate y in order to demonstrate that the critical layer is not too thin and that the vorticity's peak is shallow, as postulated earlier. As the figure illustrates, the vorticity peaks of the plane fundamental and oblique subharmonic waves coincide at $\theta = 60°$. Thus within the concept of nonlinearity being important in the critical layer, $\theta = 60°$ represents the optimum configuration for interaction. Therefore subharmonic resonance is maximum at $\theta = 60°$.

At other obliqueness angles the two critical layers overlap less because the two critical points are different. As θ decreases from $60°$, the critical point of the oblique waves moves closer to the wall but that of the plane wave is independent of θ. The peak vorticity of the oblique waves is thus subjected to a weaker vorticity of the plane wave. Therefore the interaction is weaker at lower obliqueness angles (lower spanwise wavenumbers). This can also be seen by noting that for the oblique waves the fundamental-subharmonic interaction term in the amplitude (eq. (5.1)) or in the vorticity (eq. (5.6)) is proportional to $\sin^2\theta$, which decreases with decreasing θ. In the limit of $\beta = 0$ ($\theta = 0°$) the two vorticity peaks are farther apart and the vorticity of the subharmonic becomes negligible, explaining the vanishing interaction in the limit of $\beta = 0$. As β increases beyond $60°$, the oblique waves' vorticity increases but the peak moves away from that of the plane fundamental wave. The peak vorticity of the oblique waves is thus subjected to a weaker vorticity of the plane wave, which leads to a weaker interaction. In the limit of $\beta \to \infty$ the two critical layers are farther apart and therefore, within the framework of critical-layer nonlinearity, the nonlinear interactions become negligible.

The dependence of subharmonic resonance on the spanwise wavenumber is thus explained by the overlapping of the two critical layers. The strongest interaction takes place when the two layers coincide. The interaction diminishes as the two layers grow apart when θ deviates from $60°$. This also explains the existence of a range of unstable spanwise wavenumbers outside of which the interactions cannot take place because the two critical layers no longer overlap. This further supports the basic assumption here that nonlinear interactions are important in the critical layer. Had this not been the case, there

would be no reason for the existence of a finite range of unstable spanwise wavenumbers with a preferred one.

The results presented in figure 21 also indicate that increasing the amplitude u_{2Di} extends the range of unstable spanwise wavenumbers. This can also be explained in light of the vorticity distribution. Increasing u_{2Di} raises the level of the plane wave's vorticity. Furthermore, because of the nonlinear second square-bracketed term in the oblique waves' vorticity (eq. (5.6)), it also increases with increasing u_{2Di}. Thus, if θ is such that the interactions are weak, increasing u_{2Di} increases the vorticity of both modes, resulting in stronger interactions and hence extending the range of unstable spanwise wavenumbers.

The success of explaining the interactions at various spanwise wavenumbers from the vorticity distributions in the critical layer suggests a new condition for interaction. The equal-phase-speed requirements can be relaxed as a condition for mode interactions (Raetz, 1959, and Craik, 1971). It is replaced by the requirement that the two critical layers must overlap in order for the interaction to take place. the present results fully support Craik's (1971) theory. The requirement in Craik's resonant triad that the phase speeds must be equal arises from the hypothesis that under such conditions the two critical layers would coincide and cause strong interactions. In this regard the present CLN concept demonstrates the validity of Craik's hypothesis and puts it on a rational basis. Here the need to rely on shapes predicted by the linear solution in order to calculate the nonlinear terms in the expansion is avoided, and therefore the present theory is not restricted to infinitesimally small amplitudes. The nonlinear terms are obtained herein by actually going into the critical layer and calculating the nonlinear viscous flow. For detuned conditions nonlinearity causes the effective phase angle to lock into the optimum value for resonance. The equality of the phase speeds as a necessary condition for resonance is thus relaxed. It is replaced here by the condition that the two relatively thick critical layers must overlap in order for the interaction to take place. This leads to the broad band of unstable spanwise wavenumbers.

6. DISCUSSION AND SUMMARY

The fully interactive case of a near-resonance triad of instability waves consisting of a plane fundamental wave and a pair of symmetric subharmonic oblique waves was investigated. The development of the waves was determined by the viscous critical-layer nonlinearity (CLN). A composite expansion was formed that accounts for both the nonlinear effects and those produced by the growth of the boundary layer.

The comparisons between theory and observations confirmed the following hypothesis:

1. The remarkable agreement between theory and observations for all modes and over the linear, parametric resonance, and fully interactive regimes, as well as the comparison with the numerical simulations available for the initial stages of the development, leaves little doubt that CLN plays the key role in determining the development of the waves. This confirms the importance of CLN.

31

It also provides an avenue for subsequent investigations of other related phenomena, not only on the qualitative level, but also on the quantitative level as well.

2. A low-frequency, high-Reynolds-number scaling was adopted herein that leads to a distinct critical layer separable from the viscous wall layer, typical of the upper-branch stability structure. Goldstein & Durbin (1986) argues that at low frequencies such scaling is applicable not only to the vicinity of the upper branch, but to almost all of the Reynolds number range (except close to the lower branch). Results presented herein based on this scaling were shown to agree with observations over a wide spatial domain ranging from Reynolds numbers upstream in the linearly unstable region to farther downstream beyond the upper branch. Thus the present work indirectly shows that Goldstein & Durbin s (1986) conclusion regarding the wide range of applicability of upper-branch scaling is consistent with observations.

In addition to exhibiting features almost identical to the observed ones, the study explains the observed features and reveals new ones, which are summarized here in three groups: (1) spatial development of the waves; (2) nonlinear effects on the mode shapes and on the meanflow; and (3) the effects of spanwise wavenumbers on the interaction. It is important to remember that the waves are classified into two sets. The first is the input waves of the triad, where their development is nonlinear but their amplitudes are linear. The second set is composed of those waves that were not originally present in the linear stage but are generated by the nonlinear interactions of the input waves in the triad. The waves in this second set are characterized by frequencies and wavenumbers that may be equal to or different from those of the input waves; but most importantly their amplitudes and their development are nonlinear. This distinction between the two sets is easily made in the theory, and it is helpful in clarifying several observations.

6.1. Spatial Development of Waves

6.1.1. Nonlinear Stages of Development

6.1.1.1. Subharmonic oblique waves. - The presence of the plane wave initially causes a superexponential parametric resonance growth of the oblique waves. However, as the subharmonic continues to grow, the fully interactive stage comes into effect. The self-interaction of the oblique waves causes their saturation, which is characterized by a shallow peak. This is followed by a slow decay caused mainly by the self-interaction of the oblique waves and partly by the boundary-layer growth. Boundary-layer growth causes the loss of the parametric resonance mechanism because of the decay of the fundamental, and it also causes the linear growth rate of the subharmonic to decrease and ultimately become negative.

6.1.1.2. Fundamental wave. - A distinction is made here between the plane TS fundamental wave in the input triad and the total fundamental component. The latter is composed of the input TS plane fundamental plus other nonlinearly generated waves at the fundamental frequency. These additional waves have two-dimensional as well as three-dimensional spanwise-periodic components that

exhibit nonlinear dependence on the scaled amplitude function and were not originally present in the upstream linear regime.

6.1.1.2(a) Plane TS Fundamental Wave: Although the backreaction on the plane TS fundamental is fully accounted for herein, its amplitude was found to almost follow the linear stability theory. The backreaction is quite weak and cannot explain the experimentally observed enhancement of the fundamental frequency disturbance, which contains both the input fundamental and other nonlinearly generated waves at the fundamental frequency.

6.1.1.2(b) Nonlinear waves at fundamental frequency: Nonlinearity generates waves of nonlinear amplitudes at the fundamental frequency. The significant lowest-order nonlinear waves are produced not by the interaction of the plane wave with the oblique waves but by the self-interaction of the oblique waves. Therefore the amplitudes of these nonlinear waves are proportional to A^2. They are both two-dimensional $(\alpha,0)$ and three-dimensional spanwise periodic $(\alpha,\pm2\beta)$ and were not originally present in the upstream linear stage. The interesting feature is that they appear at a lower order than that of the input plane TS fundamental in the triad and can therefore be comparable to, if not larger than, the input plane TS fundamental. This feature has a dramatic effect on the observed fundamental disturbance. Superimposing the nonlinear waves at the fundamental frequency on the input plane fundamental enhances the net fundamental disturbance in accordance with experimental observations. The measured increase in the fundamental above the linear growth is thus not due to the backreaction but is caused by the nonlinearly generated waves at the fundamental frequency. The enhanced fundamental is not two-dimensional. The nonlinearly generated waves cause the net fundamental frequency disturbance to be three-dimensional spanwise periodic, as has recently been demonstrated in the spanwise distributions measured by Corke & Mangano (1989). The spanwise wavenumber of the calculated total fundamental is twice that of the input oblique waves.

6.1.2. Backreaction

The backreaction issue plays an important role in clarifying the mechanisms involved in the later stages of laminar-turbulent transition. The present results indicate that the backreaction of the subharmonic on the fundamental is minimal. The nonlinear effect on the amplitude of the plane fundamental is in the form A^2, A_0A^*A, and A^4, but the backreaction term A^2 cancels out. The A_0A^*A term only causes a nonlinear detuning of the plane fundamental and does not influence its modulus of amplitude. The backreaction term A^4 tends to cause a steeper decay of the input plane TS fundamental. This effect is consistent with Dal-Ferro's (1987) and Corke's (1989) experimental observations that the input plant TS fundamental decayed past the upper branch. This effect can also be detected by careful examination of the early decay stage of the fundamental in Kachanov & Levchenko's (1984) data.

The observed enhancement of the total fundamental at the streamwise location where the subharmonic peaks does not therefore result from backreaction. As already mentioned, this was clarified in Corke & Mangano's (1989) experiment. Furthermore, Kachanov (1990, private communication) has also pointed out that Kachanov & Levchenko's (1984) data do not show significant backreaction on the plane fundamental wave. The enhancement in the net fundamental is caused

not by the backreaction but by the nonlinear waves generated at the fundamental frequency by means of the self-interaction of the oblique waves, as outlined in §3.1.2.2.

In fact this conclusion extends the range of validity of the linear secondary stability analysis (Herbert, 1988). His basic assumption is that the plane fundamental is the dominant mode so that it is not influenced by the interaction with the oblique subharmonic. This is obviously true if the oblique mode is much smaller than the plane mode. But the validity of such an assumption might be questioned when the oblique mode becomes comparable to or greater than the plane mode. Nevertheless the present analysis indicates that even when the oblique mode is larger than the plane mode the backreaction is still minimal. Therefore for all amplitudes the plane mode can be regarded as if it follows the linear stability theory. Thus the basic assumption in the secondary stability analysis is valid not only when the oblique mode is much smaller than the plane mode, but also when it is much larger. The secondary stability analysis can therefore be extended to higher amplitudes of the oblique waves, but then the important self-interaction of the oblique waves and the distortion of the mean flow must be accounted for.

6.1.3. Effect of Initial levels on Development and Saturation of Waves

The initial parametric resonance growth rate of the subharmonic is independent of its own initial level but increases exponentially with the initial level of the fundamental. The location of the peak moves upstream when the initial level of either the subharmonic or the fundamental is increased. Nevertheless the level of the subharmonic peak is independent of its own initial level. At moderate initial levels of the fundamental u_{2Di} the level of the subharmonic peak increases with u_{2Di}. Higher levels of u_{2Di} cause the increase in the subharmonic peak to slow down and to reach saturation, as indicated in CM's data.

The plane TS fundamental wave initially follows the linear theory in the parametric resonance stage, and its growth rate in this stage is therefore independent of the initial level of either the fundamental or the subharmonic. Raising the initial level of the subharmonic has little effect on the fundamental in the fully interactive stage. But raising the initial level of the fundamental increases the peak level of the subharmonic, enhancing the backreaction on the fundamental. Thus the fundamental decays sooner and at steeper rates with increasing u_{2Di}. Careful examination of KL's data in the decay stage reveals a similar trend.

6.1.4. Location of Resonance

The subharmonic parametric resonance growth rate was shown to be proportional not only to the amplitude of the fundamental, but also to the cubed Reynolds number. This explains why subharmonic resonance was observed to occur not far upstream of but in the vicinity and downstream of the upper branch. Furthermore dependence solely on the amplitude of the fundamental would have caused the subharmonic maximum growth rate to occur right at the upper branch where the fundamental is maximum. But experiments (Corke & Mangano, 1989; and Corke, 1989) indicate a shift in the subharmonic maximum

34

growth rate to a region downstream of the upper branch. This phenomenon has not been fully explained heretofore. Now, however, the resonance mechanism has also been shown to be explicitly dependent on the Reynolds number; this dependence explains the occurrence of the maximum growth rate downstream of not at the upper branch.

6.1.5. Nonlinear Phase Locking

It is now well known that in free shear flows the initial phase difference between the fundamental and the subharmonic can result in either growth or suppression of the subharmonic (Zang et al., 1985; Mankbadi, 1985, 1986; and Monkewitz, 1988). But the situation is different for boundary layers. For perfect tuning the optimum initial phase difference $\psi_{ei} = \psi_0 - 2\tilde{\psi}$ is $3\pi/2$ for maximum subharmonic growth rate. However, except in a narrow window around $\psi_{ei} = \pi/2$, resonance occurs for all other initial phases with almost the same strength as in the optimum ψ_{ei} case. If ψ_{ei} is close to $\pi/2$, the subharmonic initially suffers a sharp decay. But subsequently nonlinear phase locking of ψ_e to the optimum value occurs. This allows resonance to occur for $\psi_{ei} = \pi/2$ as well, but farther downstream. The subharmonic ultimately reaches a peak level that is independent of ψ_{ei}. Moreover the initial suppression at $\psi_{ei} = \pi/2$ is drastically reduced with infinitesimal detuning, which is inadvertently present in real life. Thus because of imperfection in tuning and because it is restricted to a narrow window, the subharmonic suppression at $\psi_{ei} = \pi/2$ is hardly detected in experiments. The net outcome is that subharmonic resonance depends on ψ_{ei} but only weakly. This is consistent with Saric et al.'s (1984) data as well as with the finding of Corke (1990, private communication) that ψ_{ei} has little effect on resonance.

6.1.6. Effect of Wave Number Detuning

Wavenumber detuning has no effect on the plane wave's moduli of amplitude. Large detuning delays the nonlinear phase locking and moves the location of resonance farther downstream (longer fetch). This is consistent with KL's observation as well as with Saric et al.'s (1984) comments. With detuning the subharmonic reached almost the same peak as that of the perfectly tuned case, but further downstream. This explains KL's finding that resonance can occur in a broad band of frequencies around the subharmonic value.

6.1.7. Strong Dependence on Frequency Parameter

The present results indicate that the growth rate strongly increases with the dimensionless frequency F^* in the parametric resonant stage. Available experimental data on boundary-layer transition qualitatively confirm this trend. The lower frequency domain is technologically important, but it may not be accessible to either experimental or numerical investigation, making the present results even more important.

This strong frequency dependence explains the success of the present analysis in predicting results in broad agreement with observations. The present asymptotic analysis becomes exact when the small frequency parameter goes to zero, but it is still valid and accurate at small finite F^*. Because the

parametric resonance mechanism is quite weak at higher frequencies, the resonance phenomena is significant only at the low-frequency domain where the present analysis achieves its greatest accuracy. The low-frequency asymptotic approach adopted herein is therefore applicable to the entire frequency range of observable resonance.

6.2. Nonlinear Effects on Transverse Profiles

The self-interaction of the oblique waves as well as their interaction with the plane TS fundamental wave generates several oscillating and non-oscillating nonlinear components. The present theory fully accounts for these nonlinearities, which not only contribute to the nonlinear development of amplitudes in the input triad, but also modify the transverse shapes of the modes and of the mean flow.

6.2.1. Mode Shapes

Nonlinearity modifies the transverse profiles of both the plane fundamental and oblique subharmonic modes. This nonlinear distortion is restricted to a small region centered around the critical point. The resulting mode shapes scale with Reynolds number and frequency and are in good agreement with the corresponding measurements.

6.2.2. Mean Flow

The upstream mean flow has a Blasius profile, the nonlinear self-interaction of the oblique waves produces significant mean-flow distortion with spanwise wavenumbers of 0 and 2β. This modifies the mean flow in two basic ways:

(1) Nonlinearity creates a kink in the mean flow around the critical point. The mean flow is enhanced beneath the critical point and is reduced above it. This changes the mean flow from a Blasius profile toward a fuller turbulent type of profile, in accordance with experimental observations.

(2) Nonlinearity causes the originally two-dimensional mean flow to become three-dimensional spanwise periodic. The wavenumber of this periodicity is twice that of the input oblique waves and accounts for the observed spanwise variation in boundary-layer thickness (Corke & Mangano, 1989). Thus during transition nonlinearity causes the initially two-dimensional, laminar boundary-layer profile to evolve into a three-dimensional, turbulent-like one. This mean-flow distortion influences the wave development and should therefore be considered in deriving the amplitude equtions, as is done herein.

6.3. Interaction at Various Spanwise Wavenumbers

The results discussed previously pertain to an obliqueness angle θ of 60°, which corresponds to the exact resonance condition. Experimental observations and numerical simulations indicate that subharmonic maximum growth rate

occurs at a "preferred" spanwise wavenumber β_p corresponding to an obliqueness angle θ of about $60°$, as the present analysis suggests. But the near resonance, which can also occur over a range of obliqueness angles near $60°$, can be accounted for by including a detuning factor and considering the variation of the wave speeds with the obliqueness angle, as done in §5. The predicted development of the subharmonic and the reduction in the growth rates, as well as the range of unstable spanwise wavenumbers, are in good agreement with experimental and numerical results. The analysis also indicates that there is no interaction between plane fundamental and plane ($\beta = 0$) subharmonic waves. Thus the vortex pairing that has been observed in free shear flows is suppressed in boundary layers. Other features of the near-resonance interactions are discussed here.

6.3.1. "Preferred" Spanwise Wavenumber

The appearance of subharmonics at small or large spanwise wavenumbers, such as in Saric et al.'s (1984) experiment, is explained by the CLN concept without the need to distinguish between a Craik or a Herbert type of mechanism. The subharmonic total growth rate is governed by both the linear and parametric resonance mechanisms. The observed "preferred" spanwise wavenumber follows from the dependence of these two mechanisms on (1) the Reynolds number and (2) the initial level of the plane wave, u_{2Di}.

(1) The present analysis indicates that the peak spanwise wavenumber increases with Reynolds number. The excitation in Saric et al.'s (1984) experiment was introduced at a higher Reynolds number than in other related experiments. This allowed resonance to occur at a higher spanwise wavenumber, provided that u_{2Di} was large enough.

(2) The present analysis indicates that the subharmonic can be observed for any $\beta \leq = \beta_p$ at low u_{2Di} and for any $\beta = \geq \beta_p$ at higher u_{2Di}. Therefore as in Corke & Mangano (1989) and in Spalart & Yang (1987) the spanwise wavenumber of the most amplified subharmonic would depend on $u_{3Di}(\beta)$. In Saric et al.'s (1984) experiment the oblique subharmonic was not "controlled" but arose from the background disturbance, where u_{3Di} varied randomly with β.

6.3.2. Vorticity Distribution

The dependence of the resonance mechanism on the spanwise wavenumber is related to the vorticity distribution in the critical layers. Maximum interaction occurs when the two critical layers coincide and diminishes when the critical layers move apart. This leads to the following features:

(1) The "preferred" spanwise wavenumber occurs at $\theta = 60°$, where the two critical layers coincide. The peak subharmonic vorticity is then subjected to the peak of the fundamental vorticity, which causes particularly strong interactions.

(2) As θ deviates from 60°, the overlapping of the critical layers is reduced and the peak subharmonic vorticity is subjected to off-peak fundamental vorticity, leading to a weaker interaction.

(3) This also explains the existence of a range of unstable spanwise wavenumbers outside of which the interactions do not take place because the two critical layers no longer overlap.

(4) There is no interaction between plane fundamental and plane subharmonic ($\theta = 0$) waves because the critical layers do not overlap.

(5) Increasing the initial level of the fundamental u_{2Di} enhances the vorticity of all modes, causing a stronger interaction and a wider range of unstable spanwise wavenumbers at higher u_{2Di}.

The spanwise wavenumber dependence of the growth rate, the effect of u_{2Di}, and the existence of a preferred spanwise wavenumber are thus all explainable by the CLN concept. This lends further support to the importance of CLN.

6.3.3. Condition for Mode Interaction

The success of the present theory in predicting mode interactions over a wide range of spanwise wavenumbers suggests that the equal-phase-speed requirement can be relaxed as a necessary condition for mode interaction. This requirement is replaced here by the requirement that the critical layers overlap in order for mode interaction to occur. The strength of the interaction simply follows from the degree of overlapping of the two critical layers.

7. ACKNOWLEDGMENTS

APPENDIX

DETAILS OF COMPOSITE EXPANSIONS

The results presented in §2.2 pertain to the nonlinear region, where boundary-layer variations are neglected. The overall instability wave growth is dependent on both the nonlinear effects and the weakly nonparallel flow effects. In order to incorporate both effects into a single formula, the present analysis follows Goldstein & Leib (1988) in formulating the composite expansion by using the present inner nonlinear solution A_{in} and the slowly varying outer linear solution A_{out}.

The outer linear solution of the plane wave can be written as

$$A_{o,out} = A_o^o(x_2) \exp\left[\sigma^4 \int_0^x (k_o + ik_i) dx'\right] , \qquad (A.1)$$

where x_2 is the slowly varying boundary-layer variable and A_o^o is the initial amplitude at $x = 0$. Likewise, the outer linear solution of the oblique waves is given by

$$A_{out} = A^o(x_2) \exp\left[(4/5)\sigma^4 \int_0^x k_o \, dx'\right] . \qquad (A.2)$$

As x approaches the origin of the nonlinear region x_0, these outer solutions can be approximated by

$$A_{o,out} \rightarrow a_o^o e^{(k_o + ik_i)\bar{x}} = A_{o,i/o} , \qquad (A.3)$$

$$A_{out} \rightarrow a \, e^{(4/5)k_o\bar{x}} = A_{i/o} , \qquad (A.4)$$

where

$$a_o^o = A_o^o(o) \exp\left[\sigma^4 \int_0^{x_0} (k_o + ik_i) dx\right] , \qquad (A.5)$$

$$a = A^o(o) \exp\left[(4/5)\sigma^4 \int_0^{x_0} k_o \, dx\right] . \qquad (A.6)$$

39

The inner nonlinear solutions for the oblique and plane waves, given by equations (2.7), are recast in the form

$$A_{o,in} = a_o^o e^{(k_o + ik_i)\bar{x}} g_o(\bar{x}) \ , \tag{A.7}$$

$$A_{in} = a \ e^{(4/5)k_o\bar{x}} g(\bar{x}) \ , \tag{A.8}$$

where $g_o(\bar{x})$ and $g(\bar{x})$ satisfy the equations

$$\frac{dg_o}{d\bar{x}} = iM_1 \frac{\bar{R}^{4.5}}{\lambda\sqrt{\lambda}} e^{(8/5)k_o\bar{x}} gg^*g_o - iM_2 \frac{\bar{R}^6}{\lambda^2} g^3g^* e^{(16/5)k_o\bar{x}-(k_o+ik_i)\bar{x}} \ , \tag{A.9}$$

$$\frac{dg}{d\bar{x}} = \frac{3}{10} \pi \frac{\bar{R}^3}{\lambda} g_og^* e^{(k_o+ik_i)\bar{x}} - \frac{2}{5} iM \frac{\bar{R}^{4.5}}{\lambda\sqrt{\lambda}} g^2g^* e^{(8/5)k_o\bar{x}} \ . \tag{A.10}$$

Equations (A.9) and (A.10) show that as $\bar{x} \to -\infty$,

$$\frac{dg_o}{d\bar{x}} (-\infty) = \frac{dg}{d\bar{x}} (-\infty) = 0 \ . \tag{A.11}$$

Thus the inner solution for the plane and oblique waves can be approximated as $\bar{x} \to -\infty$ by

$$A_{o,in} = a_o^o e^{k_o\bar{x}} = A_{o,i/o} \ , \tag{A.12}$$

$$A_{in} = \frac{4}{5} a^o e^{k_o\bar{x}} = A_{i/o} \ . \tag{A.13}$$

The composite solutions are given according to van Dyke (1975) by

$$A_c = \frac{A_{in}A_{out}}{A_{i/o}} \ . \tag{A.14}$$

The subscript c denotes the composite expansion. Substituting equations (A.1) to (A.4), (A.7), and (A.8) into equation (A.14) gives

$$A_{o,c} = A_o^o(0)g_o \ \exp\left[\sigma^4\int_0^x (k_o+ik_i)dx\right] = A_o(x) \ , \tag{A.15}$$

$$A_c = A^O(0)g \exp\left[\sigma^4 \int_0^x (k_0 + ik_i)dx\right] = A(x) , \qquad \text{(A.16)}$$

with $A(x)$, and $A_0(x)$ satisfying the equations

$$\frac{dA}{dx} = \sigma^4\left(\frac{4}{5} k_0 A + \frac{3}{10} \pi \frac{\bar{R}^3}{\lambda} iA^*A_0 - \frac{2}{5} iMA^2A^* \frac{\bar{R}^{4.5}}{\lambda\sqrt{\lambda}}\right) , \qquad \text{(A.17)}$$

$$\frac{dA_0}{dx} = \sigma^4\left[(k_0 + ik_i)A_0 + iM_1 \frac{\bar{R}^{4.5}}{\lambda\sqrt{\lambda}} A_0 AA^* - iM_2 \frac{\bar{R}^6}{\lambda^2} A^*A^3\right] . \qquad \text{(A.18)}$$

For convenience, the subscript c has been dropped in equations (A.17) and (A.18) and in what follows.

Recalling that x is the dimensional streamwise coordinate normalized by the local boundary-layer thickness $\delta(x)$, the variation of the boundary-layer thickness is now taken into consideration. Let x_w be the location of the origin of the disturbance (e.g., a vibrating wire) with respect to the leading edge of the flat plate. According to Hinze (1975), the boundary-layer variation is given by

$$\frac{\delta}{\delta_0} = \sqrt{x^+ + 1} , \qquad \text{(A.19)}$$

where

$$x^+ = \frac{x}{x_w} . \qquad \text{(A.20)}$$

Equations (A.17) and (A.18) can then be written in terms of the Reynolds number R as

$$\frac{dA}{dR} = \sigma^4\left(1 + \frac{R_i^2}{R^2}\right)\left(\frac{4}{5} k_0 A + \frac{3}{10} \pi \frac{\bar{R}^3}{\lambda} iA^*A_0 - \frac{2}{5} iM \frac{\bar{R}^{4.5}}{\lambda\sqrt{\lambda}} A^2A^*\right) , \qquad \text{(A.21)}$$

$$\frac{dA_0}{dR} = \sigma^4\left(1 + \frac{R_i^2}{R^2}\right)\left[(k_0 + ik_i)A_0 + iM_1 \frac{\bar{R}^{4.5}}{\lambda\sqrt{\lambda}} A_0 AA^* - iM_2 \frac{\bar{R}^6}{\lambda^2} A^*A^3\right] . \qquad \text{(A.22)}$$

APPENDIX B

NUMERICAL PROCEDURE FOR SOLVING THE AMPLITUDE EQUATIONS

The amplitude equations are obtained by solving the set of three simultaneous initial-value real equations (2.11) in the scaled amplitudes and the effective phase-difference angle. The scaled initial amplitudes can be related to the unscaled ones through equation (2.10) or can be related to the streamwise velocity component in the critical layer through equation (4.1), coupled with a similar equation for the fundamental. The phase angle ψ_{eo} is taken $3\pi/2$ unless otherwise stated (see §3.5). The small-frequency parameter σ appearing in equations (2.11) is obtained from the dimensionless frequency F^* through equation (2.1b). The coefficients in the equations are functions of the scaled Reynolds number which is related to its initial value through equation (A.19).

Given the initial unscaled Reynolds number, the scaled one could be obtained directly from equation (2.1a), but as in Bodonyi & Smith (1981), this would lead to underestimating the asymptotic <u>linear</u> upper branch. Bodonyi & Smith (1981) have suggested that an origin shift d is applied to the unscaled Reynolds number in order for the asymptotic upper-branch Reynolds number to match the experimentally determined one. They have shown that the gradual trend of the asymptotic results does seem to be toward the experimental ones as the number of terms in the asymptotic series representing the wavenumbers is increased (see also Hultgren, 1987). Rather than calculating additional cumbersome terms in the asymptotic expansion of the linear neutral stability curve, they have pointed out that "an origin shift is permissible in the values of the Reynolds number from the asymptotic theory, as far as that theory has been taken;" i.e., the result obtained from setting the linear growth rate in equation (2.7c) to zero and using (2.1) "remains valid even when R is replaced by $R + d$, where d is an $O(1)$ origin shift in R, and the origin shift accounts for much of the apparent discrepancy." Further discussions are given in Bodonyi & Smith (1981) regarding this issue and the accuracy of the experimentally determined upper branch.

This issue that the asymptotically obtained linear upper branch's Reynolds number is underestimated has little or no bearing on the comparison with experiments given in the present work. The reason is that the resonance phenomena occurs in the vicinity of the upper branch where the linear growth rate is quite small. The subharmonic growth is dominated by the nonlinear effects obtained herein, and, therefore, the linear growth rate and the precise location of the upper branch is not a significant issue here.

At any rate, the errors resulting from underestimating the upper branch are eliminated in the results presented herein by shifting the asymptotic upper branch, as was done by Bodonyi & Smith (1981). Thus in using the measured initial Reynolds number to calculate the scaled one, an origin shift is applied to the measured initial Reynolds number such that the asymptotic upper branch matches the measured one, i.e.,

$$R_{up} = d + \frac{\bar{R}_{up}}{\sigma^{10}} . \tag{B.1}$$

The initial scaled Reynolds number is thus given by

$$\bar{R}_i = \bar{R}_{up} + \sigma^{10}(R_i - R_{up}) \tag{B.2}$$

where $\bar{R}_{up} = 0.1537$ and $\bar{R}_{up}$ is the experimental or the Orr-Sommerfeld value.

The initial-value problem, consisting of the ordinary differential equations (2.11), are solved numerically using the IVPRK subroutine of the IMSL libraries. IVPRK finds an approximation to the solution of first-order differential equations, keeping the global error proportional to a specified tolerance, using Runge-Kutta formulas of order five and six. Rather than working with the amplitude equations directly, the equations were written in terms of the logarithm of the amplitude in order to minimize the errors resulting from the excessive growth of the subharmonic.

REFERENCES

Corke, T.C. and Mangano, R.A. 1987 Transition of a boundary layer: controlled fundamental-subharmonic interactions. Fluid Dynamics Center Rept. No. 87-1, Illinois Institute of Technology, Chicago, Illinois.

Corke, T.C. 1989 Effect of controlled resonant interaction and mode detuning on turbulent transition in boundary layers. Third IUTAM Symposium on Laminar to Turbulent Transition, Toulous, France, September 1989.

Corke, T.C. and Mangano, R.A. 1989 Resonant growth of three-dimensional modes in transitioning Blasius boundary layers. J. Fluid Mech. 209, 93-150.

Corke, T.C. 1990 Private communication.

Craik, A.D.D. 1971 Non-linear resonant instability in boundary layers. J. Fluid Mech. 50, 393-413.

Craik, A.D.D. 1985 Resonant interactions in shear flows. In Laminar-Turbulent Transition, (ed., V.V. Kozlov), pp. 1-8, Springer.

Crouch, J.D. 1988 The nonlinear evolution of secondary instabilities in boundary layers. Ph.D. Thesis, Virginia Polytechnique Institute and State University, Blacksburg, VA.

Dal-Ferro, P.R. 1987 Later stages of transition in three-dimensional seeded boundary layers. M.S. Thesis, Illinois Institute of Technology, Chicago, IL.

Fasel, H.F., Rist, U., and Konzelmann, U. 1990 Numerical investigations of the three-dimensional development in boundary-layer transition, AIAA J. 28, 29-37.

Goldstein, M.E. and Durbin, P.A. 1986 Nonlinear critical layers eliminate the upper branch of spatially growing Tollmien-Schlichting waves. Phys. Fluids 29, 2344-2345.

Goldstein, M.E. and Leib, S.J. 1988 Nonlinear roll-up of externally excited free shear layers. J. Fluid Mech. 191, 481-515.

Herbert, Th. 1984 Analysis of the subharmonic route to transition in boundary layers. AIAA Paper 84-0009.

Herbert, T., Bertolotti, F.P., and Santos, Q.R. 1987 Floquet analysis of secondary instability in shear flows. In Stability of Time-Dependent and Spatially Varying Flows (ed., D.L. Dwoyer, N.Y. Hussaini), pp. 43-57, Springer-Verlag.

Herbert, Th. 1988 Secondary instability of boundary layers. In Annual Review of Fluid Mechanics, Vol. 20, (eds., J.L. Lumley, M. van Dyke, & H.L. Reed), pp. 487-526, Annual Reviews Inc.

Hinze, J.G. 1975 Turbulence, 2nd edition McGraw-Hill, New York.

Ho, C.M. and Huang, L.S. 1982 Subharmonics and Vortex merging in mixing layers. J. Fluid Mech., 119, 443-473.

Hultgren, L.S. 1987 Higher eigenmodes in the Blasius boundary-layer stability problem. Phys. Fluids 30, 2947-2951.

Kachanov, Yu.S. and Levchenko, V.Ya. 1984 The resonant interaction of disturbances at laminar-turbulent transition in a boundary layer. J. Fluid Mech. 138, 209-247.

Kachanov, Yu.S. 1987 On the resonant nature of the breakdown of a laminar boundary layer. J. Fluid Mech. 194, 43-74.

Kachanov, Yu.S. 1990 Private correspondence.

Mankbadi, R.R. 1985 On the interaction between fundamental and subharmonic instability waves in a turbulent round jet. J. Fluid Mech. 160, 385-419.

Mankbadi, R.R. 1986 The effect of phase-difference on the spreading rate of a jet. AIAA J. 24, 1941-1948.

Mankbadi, R.R. 1991 A critical-layer theory for boundary-layer transition. Part I: Nonlinear Dynamics, In preparation for J. Fluid Mech.

Monkewitz, P.A. 1988 Subharmonic resonance, pairing and shredding in the mixing layer. J. Fluid Mech. 188, 223-252.

Nayfeh, A.H. and Bozatli, A.N. 1979 Secondary instability in boundary-layer flows. Phys. of Fluids 22, 805-813.

Raetz, G.S. 1959 A new theory of the cause of transition in fluid flows. Northrop Corp. Rep. NOR-59-383, Hawthorne, CA.

Santos, G.R. and herbert, T. 1986 Combination resonance in boundary layers. Bull. Am. Phys. Soc. 32, 1718-1725.

Saric, W.S., Kozlov, V.V., and Levchenko, V.Ya. 1984 Forced and unforced subharmonic resonance in boundary layer transition. AIAA Paper 84-0007.

Saric, W.S., and Thomas, A.S.W 1984 Experiments on the subharmonic route to turbulence in boundary layers. In Turbulence and Chaotic Phenomena in Fluids (ed., T. Tatsumi), pp. 117-22, North Holland.

Schlichting, H. 1955 Boundary Layer Theory. McGraw-Hill.

Spalart, P.R. and Yang, K.-S. 1987 Numerical study of ribbon-induced transition in Blasius flow. J. Fluid Mech. 178, 345-365.

van Dyke, M.D. 1975 Perturbation Methods in Fluid Mechanics. Parabolic Press.

Zaman, K.B.M.Q. and Hussain, A.K.M.F. 1980 Vortex pairing in a circular jet under controlled excitation, part I: General jet response. J. Fluid Mech. 101, 449-491.

Zang, T.A. and Hussani, M.Y. 1985 Numerical experiments on the stability of controlled shear flows. AIAA Paper 85-1698.

Zang, T.A. and Krist, S.E. 1989 Numerical experiments on stability and transition in plane channel flow. Theoret. Comput. Fluid Dynamics 1, 41-64.

Zhang, Y.Q., Ho, C.M., and Monkewitz, P. 1985 The mixing layer forced by fundamental and subharmonic. In Laminar-Turbulent Transition (ed., V.V. Kozlov), pp. 385-396, Springer-Verlag.
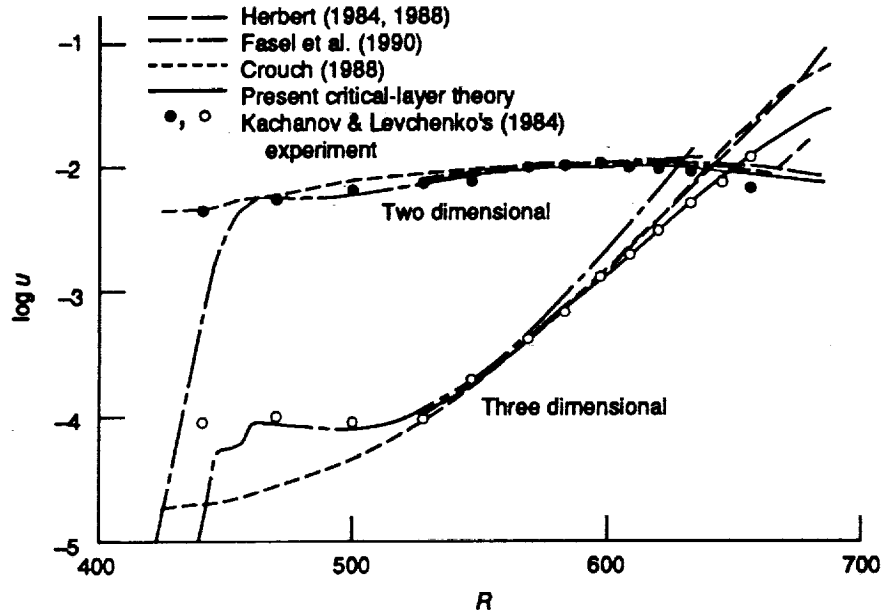
Figure 1.—Predicted development of waves compared with observation at $F^* = 124 \times 10^{-6}$ ($u_{2Di} = 10^{-2.1}$ and $u_{3Di} = 10^{-4}$).

(a) $F^* = 93 \times 10^{-6}$, ($u_{2Di} = 0.43\%$, and $u_{3Di} = 10^{-4}$).

(c) $F^* = 82.7 \times 10^{-6}$, ($u_{2Di} = 0.41\%$, and $u_{3Di} = 0.12\%$; data of Corke & Mangano (1987) in their figure 65.

(b) $F^* = 88 \times 10^{-6}$, ($u_{2Di} = 0.41\%$, and $u_{3Di} = 0.03\%$; data of Corke & Mangano (1989) in their figure 66.

(d) $F^* = 79 \times 10^{-6}$, ($u_{2Di} = 0.44\%$, and $u_{3Di} = 0.15\%$; data of Corke & Mangano (1989) in their figure 17.
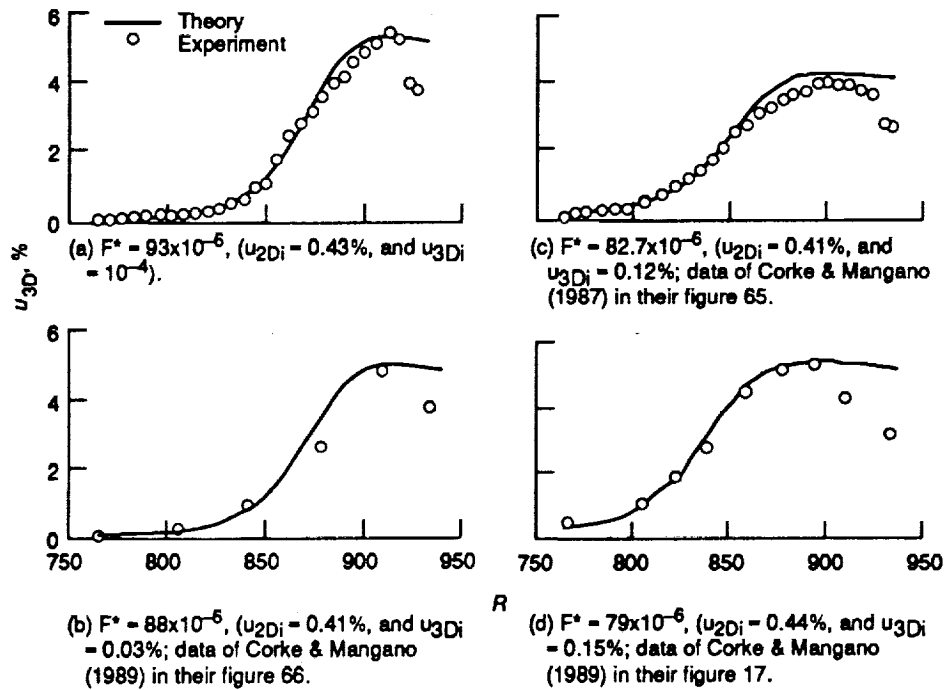
Figure 2.—Predicted subharmonic compared with experimental data of Corke & Mangano (1987, 1989).

46
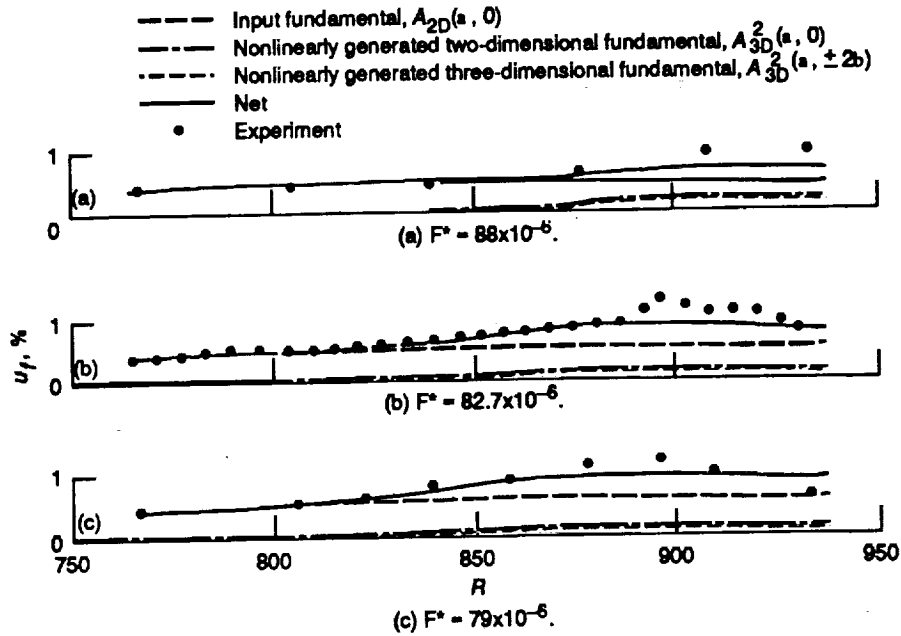
Figure 3.—Predicted plane TS input fundamental wave and nonlinearly generated waves at fundamental frequency, compared with data of Corke & Mangano (1987, 1989).

(a) Theory.

(b)Corke & Mangano's (1989) data in their figure 30.
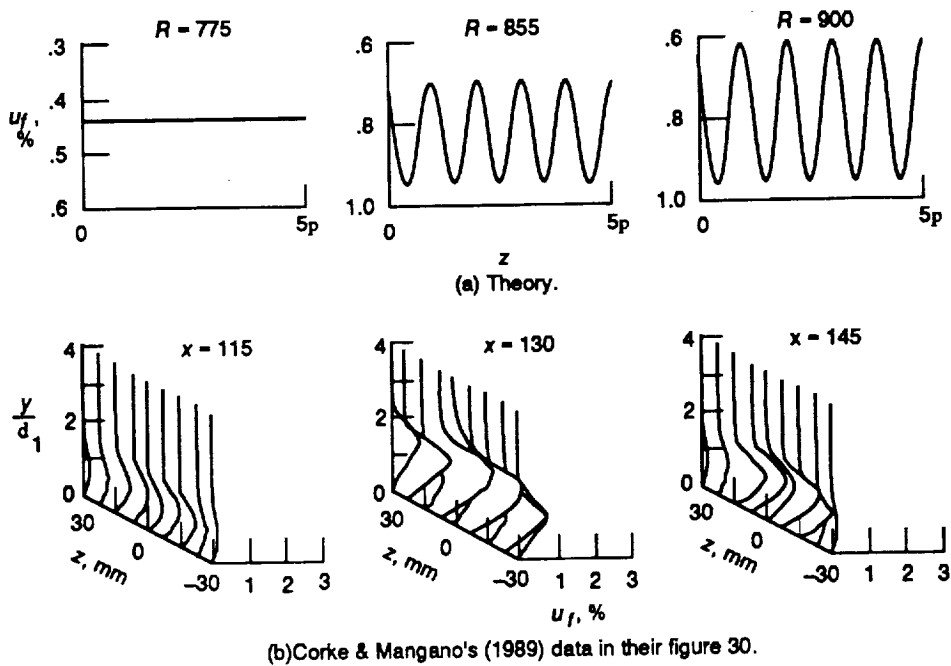
Figure 4.—Spanwise distribution of fundamental mode u-eigenfunction moduli. The enhancement in the fundamental is spanwise periodic.

(a) $F^* = 82.7 \times 10^{-6}$ (Crouch's fig. 4.23).

(b) Corke & Mangano's (1989) data in their figure 30.
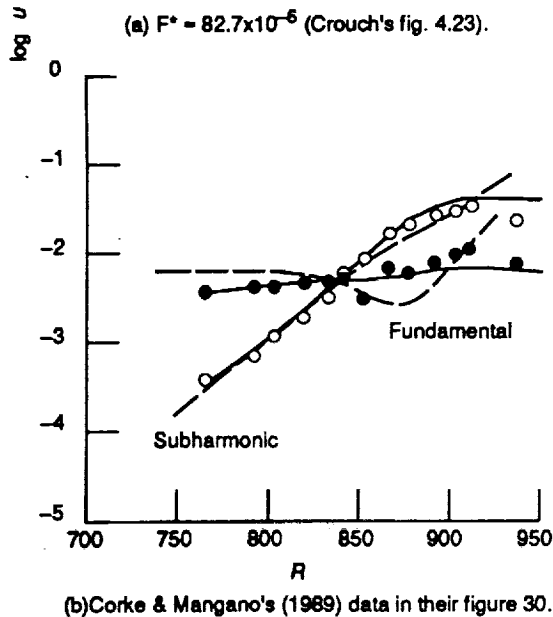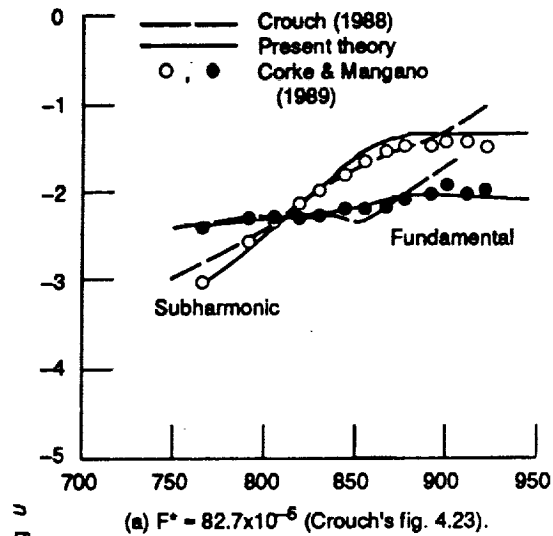
Figure 5.—Spanwise distribution of fundamental mode u-eigenfunction moduli. The enhancement in the fundamental is spanwise periodic.
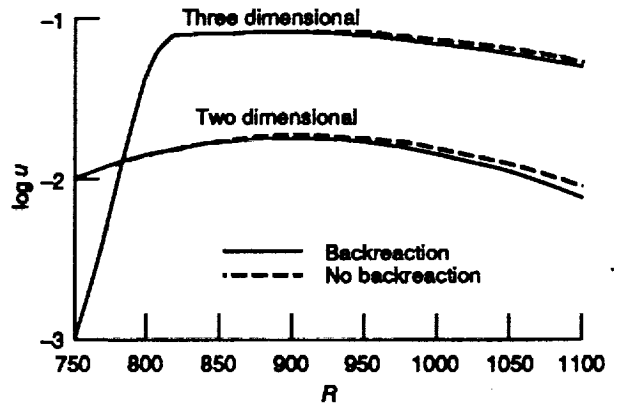
Figure 6.—Effect of backreaction on development of triad waves ($F^* = 80 \times 10^{-6}$, $u_{2Di} = 1\%$, and $u_{3Di} = 0.1\%$).
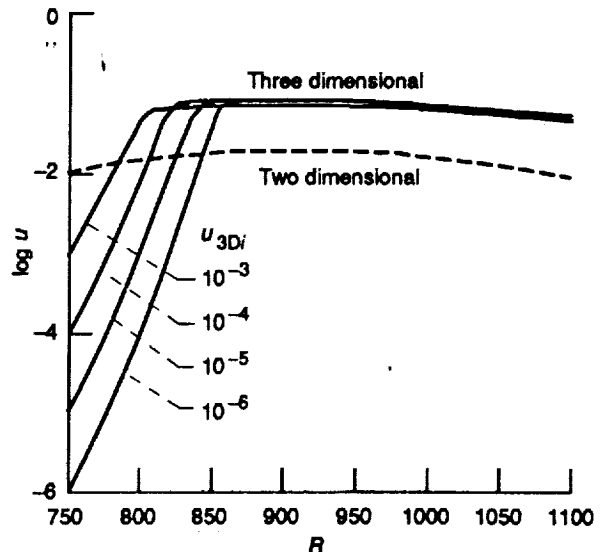
Figure 7.—Effect of initial level of subharmonic on development of triad waves ($F^* = 80 \times 10^{-6}$, $u_{2Di} = 1\%$).

48
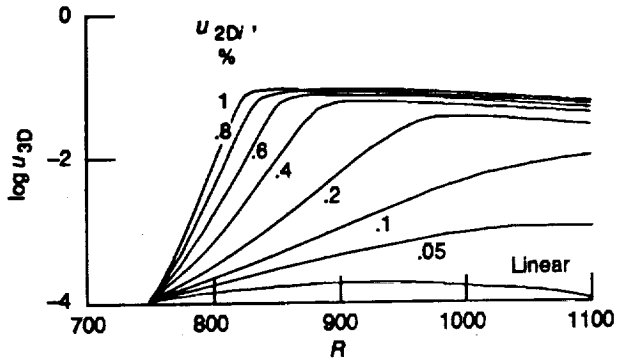
(a) Development of subharmonic ($F^* = 80 \times 10^{-6}$ and $u_{3Di} = 0.01\%$).
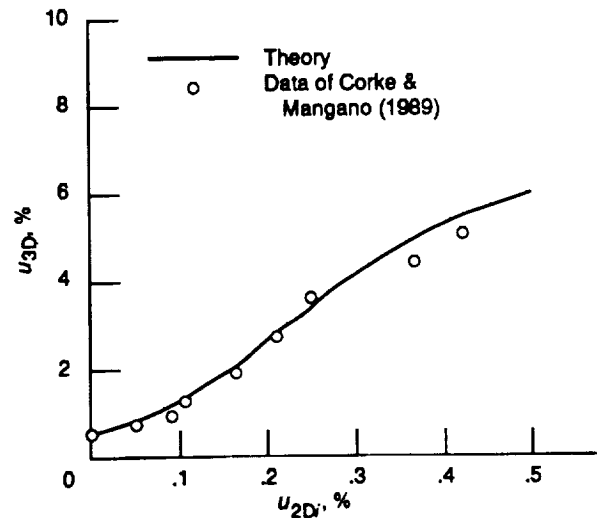
(b) Development of subharmonic ($F^* = 80 \times 10^{-6}$ and $u_{3Di} = 0.01\%$).

Figure 8.—Effect of initial level of fundamental on subharmonic.

(a) Development of subharmonic ($F^* = 80 \times 10^{-6}$ and $u_{3Di} = 0.01\%$).

	u_{2Di}, %
1	0.022
2	.163
3	.218
4	.436
5	.654
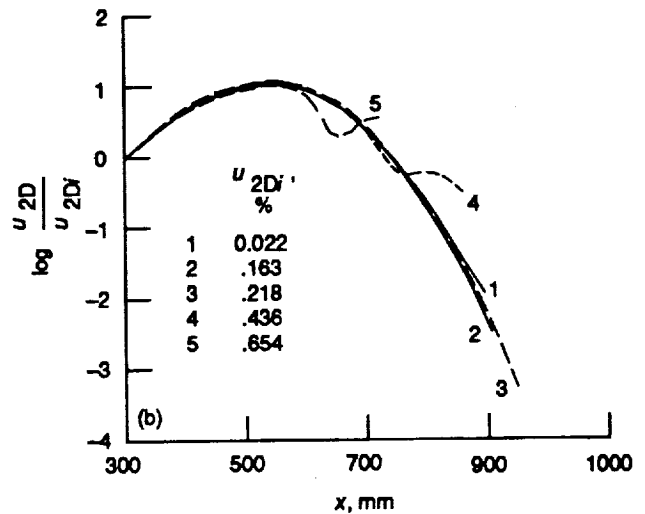
(b) Development of subharmonic ($F^* = 80 \times 10^{-6}$ and $u_{3Di} = 0.01\%$)

Figure 9.—Effect of initial level of fundamental on on its own development.
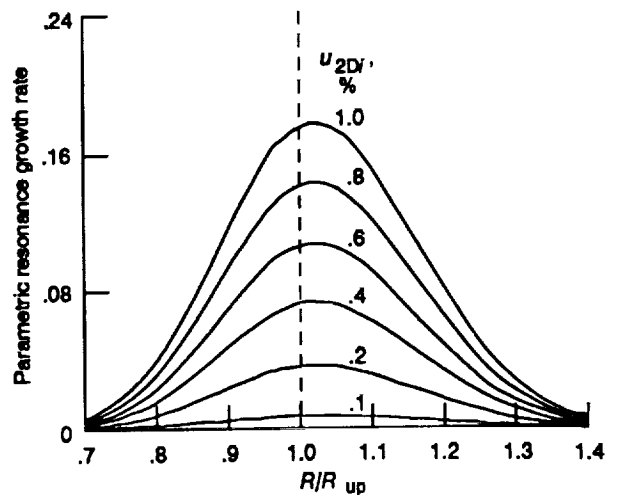
Figure 10.—Subharmonic's resonance begins to occur in the vicinity of the upper-branch neutral stability curve ($F^* = 80 \times 10^{-6}$ and $u_{3Di} = 0.01\%$).

49
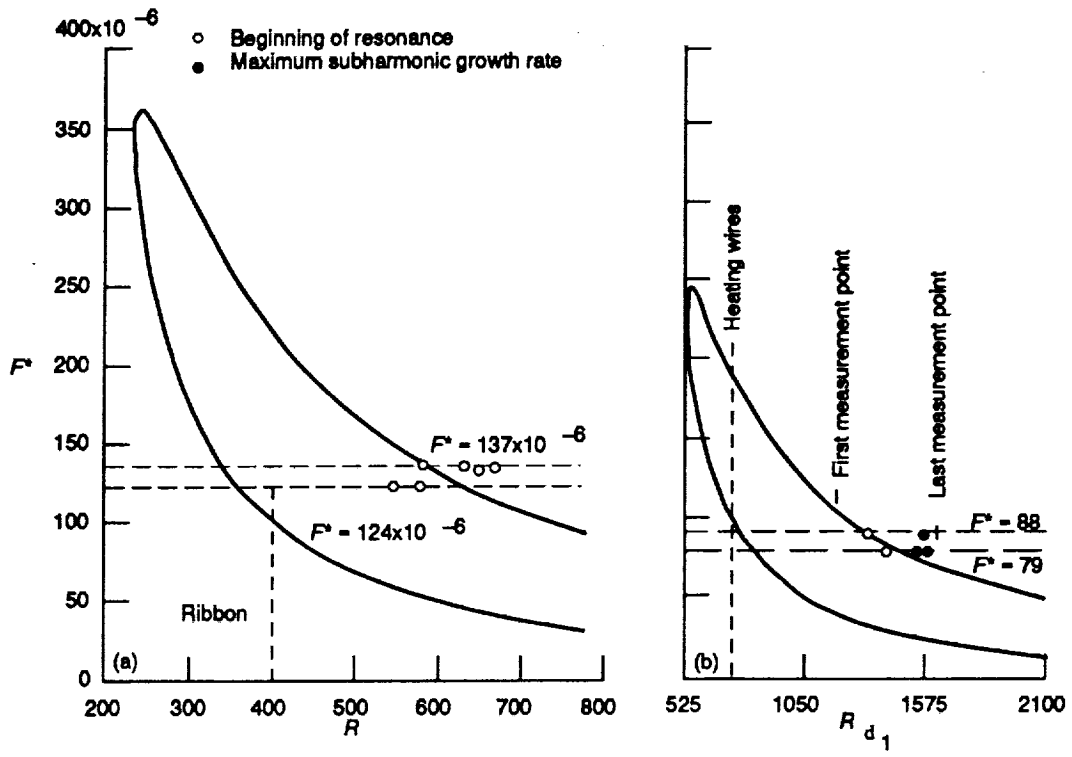
(a) Kachanov & Levchenko's (1984) data.

(b) Corke & Mangano's (1989) data.
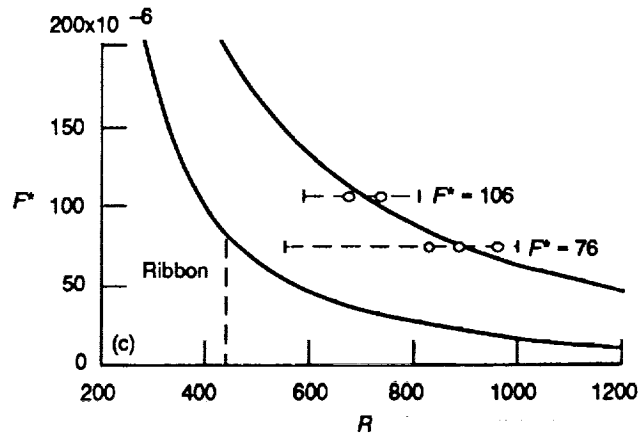
(c) Saric et al.'s (1984) data.

Figure 11.—Experimental data on location of resonance.
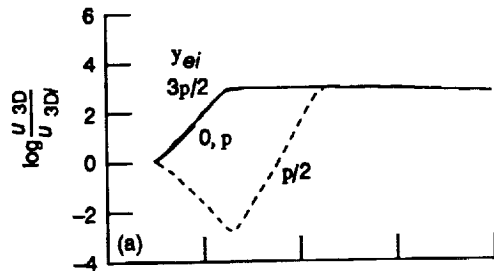
(a) Subharonic.
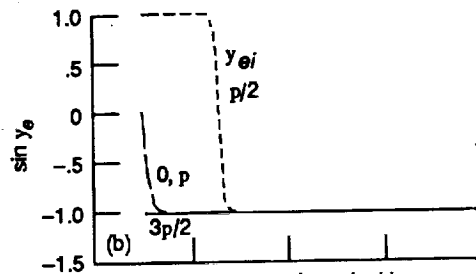
(b) Nonlinear phase locking.
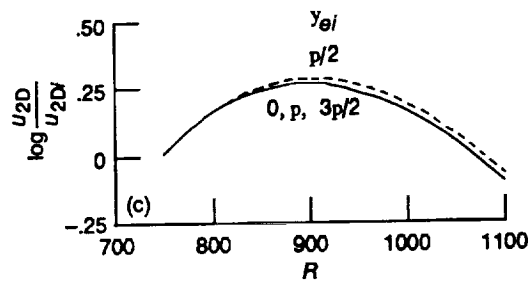
(c) Plane TS fundamental.

Figure 12.—Effect of initial phase-difference
angle $\psi_{ei} = \psi_0 - 2\bar{\psi}$ on development of waves
($F^* = 80\times10^{-6}$, $u_{2Di} = 1\%$, and $u_{3Di} = 0.01\%$).
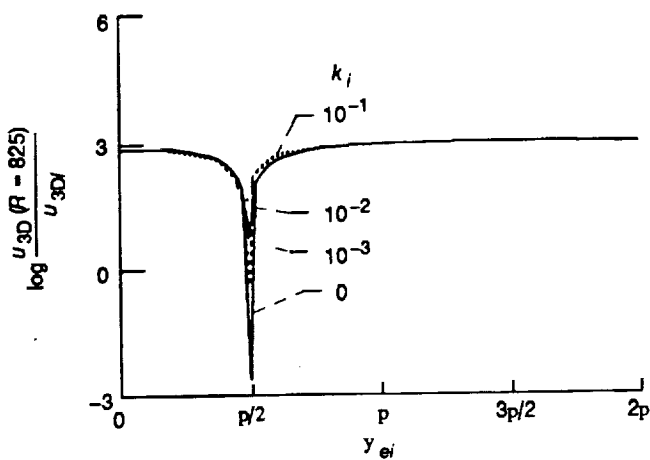
Figure 13.—Effect of initial phase-difference angle ψ_{ei} on
subharmonic at R = 825 ($F^* = 80\times10^{-6}$, $u_{2Di} = 1\%$, and
$u_{3Di} = 0.01\%$). Effect of ψ_{ei} is limited to a narrow
window around $\pi/2$ and is considerably reduced with
small detuning.
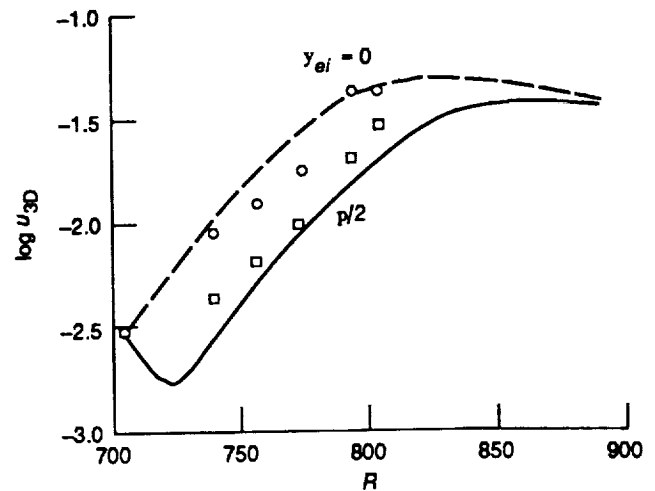
Figure 14.—Predicted amplitude of subharmonic at two
initial phases-fifference angles ψ_{ei} differing by $\pi/2$
compared with Saric et al.'s (1984) data ($F^* = 160\times10^{-6}$,
$u_{2Di} = 0.6\%$ at R = 705).

51
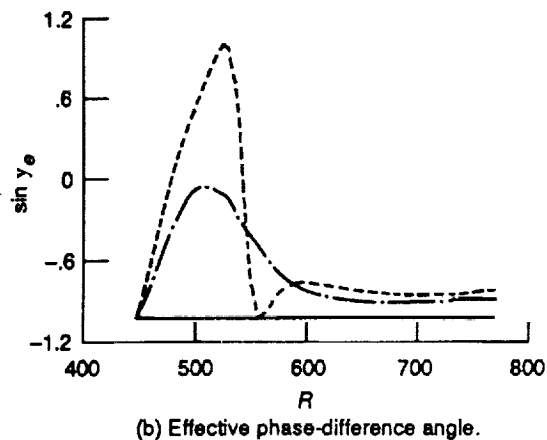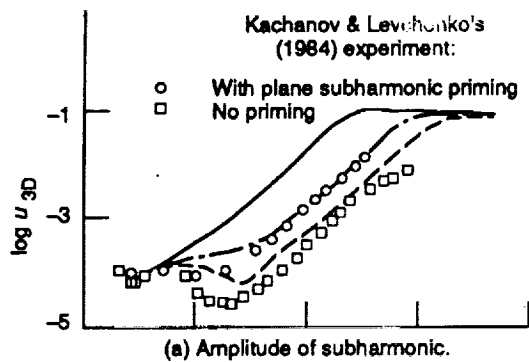
Figure 15.—Effect of wavenumber detuning at $F^* = 124 \times 10^{-6}$.

(a) Amplitude of subharmonic.

(b) Effective phase-difference angle.
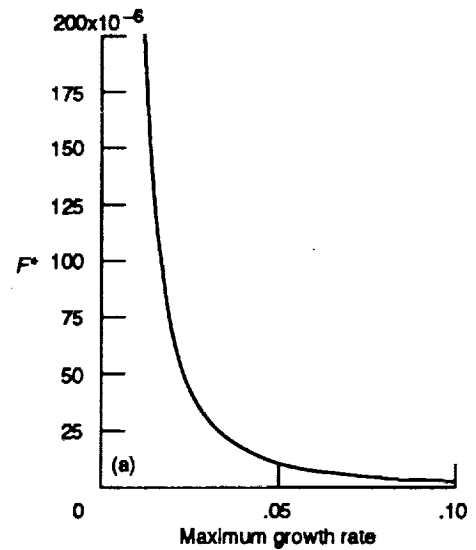
(a) Predicted maximum growth rate of subharmonic ($u_{2Di} = 0.005$, $u_{3Di} = 10^{-6}$, and $R_i = R_{up}$).

(b) Collected data of measured maximum subharmonic
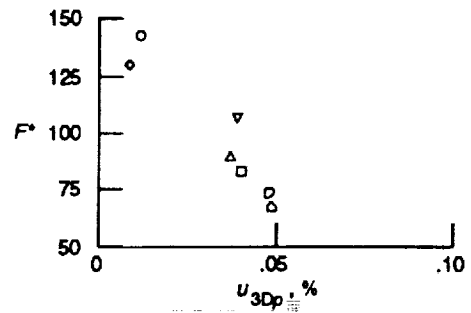
Figure 16.—Effect of frequency on maximum growth rate of subharmonic.
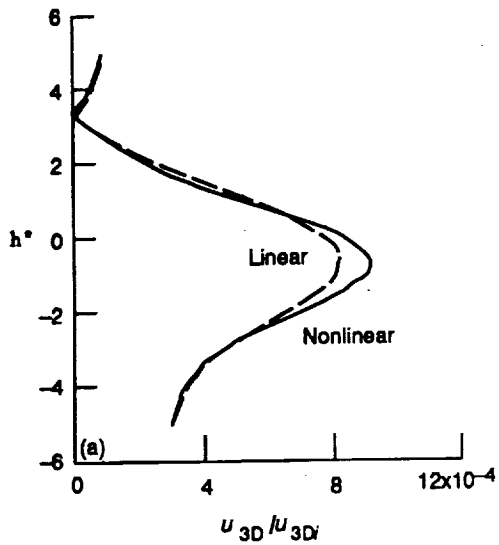
(a) Calculated linear and nonlinear profiles of subharmonic mode ($F^* = 80 \times 10^{-6}$ and $u_{2Di} = 1\%$, and $R_i = R_{up}$).
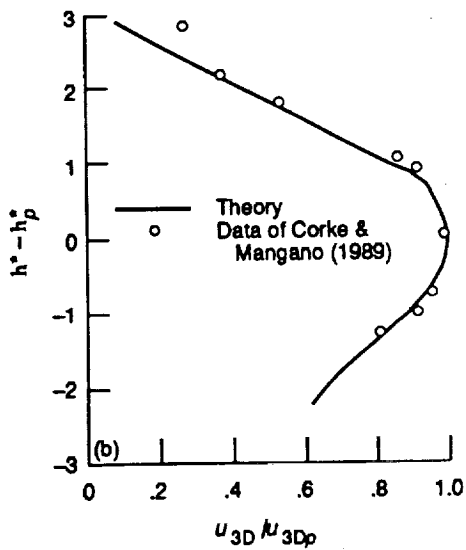
(b) Comparison between calculated and measured subharmonic's profile ($F^* = 79 \times 10^{-6}$ and $R = 840$).

Figure 17.—Modification of mode shape by nonlinearity.
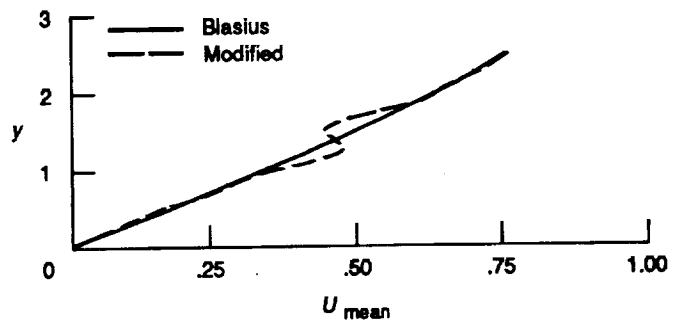
Figure 18.—Modification of mean-flow Blasius profile to a fuller turbulent type profile by nonlinearity ($F^* = 80 \times 10^{-6}$ and $R = 840$).
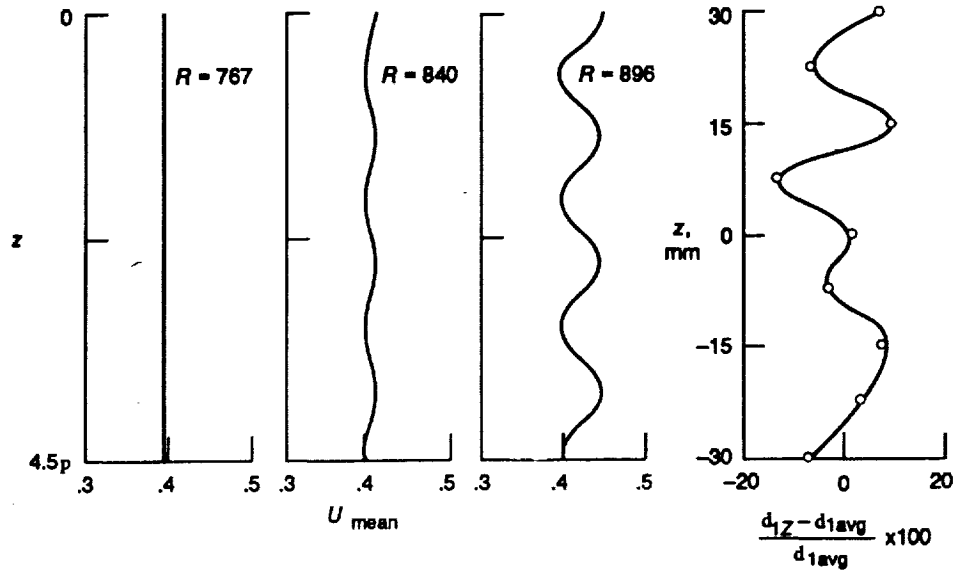
(a) Prediction of mean flow at y = 1.2.

(b) Measured displacement thickness in Corke & Mangano (1989) (their fig. 3).

Figure 19.—Modification of initially two-dimensional mean flow into a three-dimensional spanwise periodic one by nonlinearity ($F^* = 79 \times 10^{-6}$).
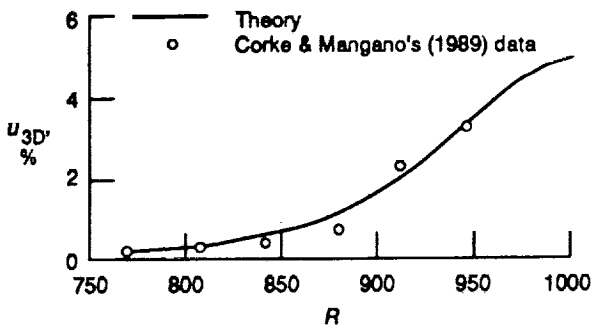
Figure 20.—Predicted subharmonic at u = 45° compared with experimental data of Cork & Mangano (1989) ($F^* = 88 \times 10^{-6}$, $u_{2Di} = 0.2\%$, and $u_{3Di} = 0.15\%$).
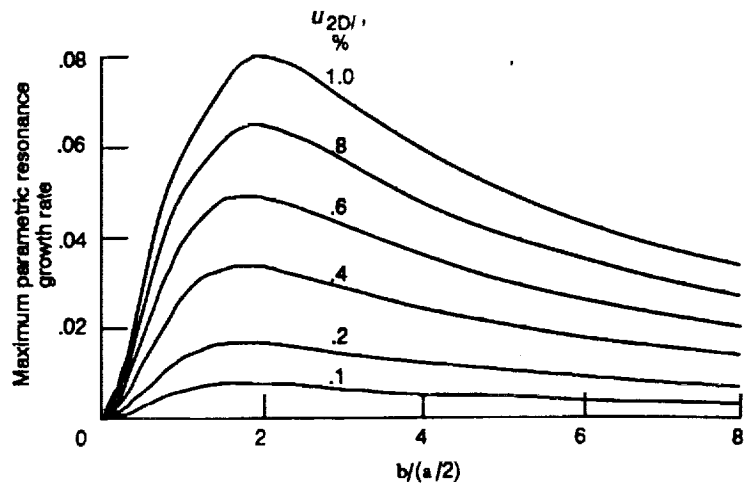

Figure 21.—Effect of spanwise wavenumber on maximum parametric resonance growth rate of subharmonic for various initial levels of plane wave ($F^* = 80 \times 10^{-6}$, $u_{3Di} = 10^{-6}$, and $R_i = 750$).
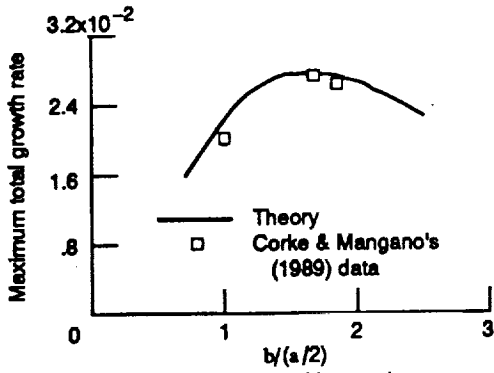
(a) Comparison with experiment.
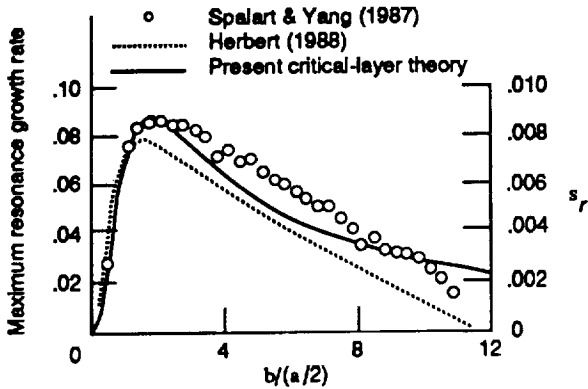
(b) Comparison with numerical investigations
($F^* = 58.8 \times 10^{-6}$, $u_{2Di} = 1.4\%$, and $R_i = 950$).

Figure 22.—Effect of spanwise wavenumber on subharmonic maximum growth rate.
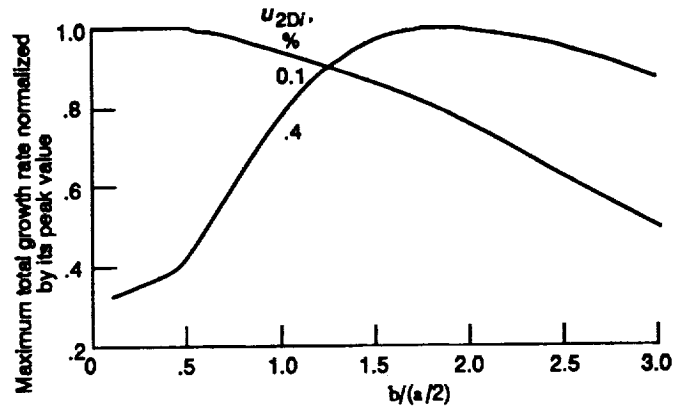

Figure 23.—Effect of low and moderately high initial levels of plane wave on preferred spanwise wavenumber ($F^* = 80 \times 10^{-6}$, $u_{3Di} = 10^{-6}$, and $R_i = 750$).
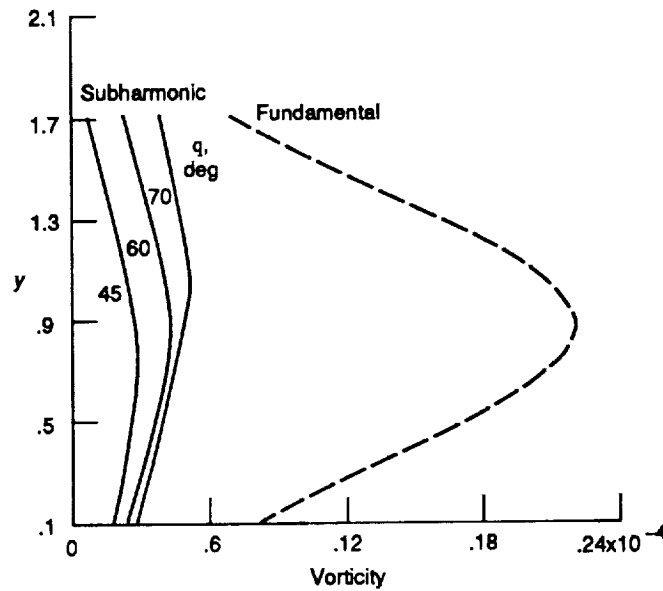

Figure 24.—Vorticity distribution in critical layers ($F^* = 80 \times 10^{-6}$, $u_{2Di} = 2\%$, $u_{3Di} = 0.01\%$, and $R_i = R_{up}$).

REPORT DOCUMENTATION PAGE

1. AGENCY USE ONLY (Leave blank)	2. REPORT DATE September 1991	3. REPORT TYPE AND DATES COVERED Technical Memorandum

4. TITLE AND SUBTITLE

Resonant Triad in Boundary-Layer Stability
Part II. Composite Solution and Comparison With Observations

5. FUNDING NUMBERS

WU-505-62-21

6. AUTHOR(S)

Reda R. Mankbadi

7. PERFORMING ORGANIZATION NAME(S) AND ADDRESS(ES)

National Aeronautics and Space Administration
Lewis Research Center
Cleveland, Ohio 44135-3191

8. PERFORMING ORGANIZATION REPORT NUMBER

E-6045-1

9. SPONSORING/MONITORING AGENCY NAMES(S) AND ADDRESS(ES)

National Aeronautics and Space Administration
Washington, D.C. 20546-0001

10. SPONSORING/MONITORING AGENCY REPORT NUMBER

NASA TM-105209

11. SUPPLEMENTARY NOTES

Responsible person, Reda R. Mankbadi, (216) 433-8569.

12a. DISTRIBUTION/AVAILABILITY STATEMENT

Unclassified - Unlimited
Subject Category 34

12b. DISTRIBUTION CODE

13. ABSTRACT (Maximum 200 words)

Numerical results are computed from the asymptotic near-resonance triad analysis of part I. The analysis considers a resonant triad of instability waves consisting of a plane fundamental wave and a pair of symmetrical oblique subharmonic waves. The relevant scaling ensures that nonlinearity is confined to a distinct critical layer. The analysis is first used to form a composite solution that accounts for both the flow-divergence and nonlinear effects. It is shown that the backreaction on the plane Tollmien-Schlichting (TS) fundamental wave, although fully accounted for, is of little significance. The observed enhancement at the fundamental frequency disturbance is not in the plane Tollmien-Schlichting wave but is caused by nonlinearly generated waves at the fundamental frequency that result from nonlinear interactions in the critical layer. The saturation of the oblique waves is caused by their self-interaction. The nonlinear phase-locking phenomenon, the location of resonance with respect to the neutral stability curve, low-frequency effects, detuning in the streamwise wavenumbers, and nonlinear distortion of the mode shapes are discussed. Nonlinearity modifies the initially two-dimensional Blasius profile into a fuller one with spanwise periodicity. The interactions at a wide range of unstable spanwise wavenumbers are considered, and the existence of a "preferred" spanwise wavenumber is explained by means of the vorticity distribution in the critical layer. Besides presenting novel features of the phenomena and explaining the delicate mechanisms of the interactions, the results of the theory are in excellent agreement with experimental and numerical observations for all stages of the development and for various input parameters.

14. SUBJECT TERMS

Stability; Transition; Boundary-layer

15. NUMBER OF PAGES
56

16. PRICE CODE
A04

17. SECURITY CLASSIFICATION OF REPORT	18. SECURITY CLASSIFICATION OF THIS PAGE	19. SECURITY CLASSIFICATION OF ABSTRACT	20. LIMITATION OF ABSTRACT
Unclassified	Unclassified	Unclassified	